The development and analysis of conductive nonwoven carbon fibre veils for electromagnetic shielding applications.

Andrew Austin
Manchester, United Kingdom
Masters By Research
January 2010

Abstract

Electromagnetic interference (EMI) is a growing problem in the modern world and as the number of devices and their operating frequencies increase so do the issues associated with EMI.
The aim of this study is to understand and quantify the main parameters that govern the Shielding Effectiveness of 'carbon fibre' based materials, in the form of nonwoven veils. Frequencies from 2.6 to 40 GHz were analysed, and it was found that the most conductive veils ($0.14 \pm 0.05\ \Omega$/sq) provided over 120dB of attenuation.

Investigations into how parameters such as fibre length, veil basis weight and metal coatings affect the shielding performance are also included.

Acknowledgements

My supervisors; Dr Mike Jeschke, Dr Mike Barker and Dr John Sharp for their commitment and support throughout the project.

Technical Fibre Products: research, technical and marketing divisions for their input, training, and experience.

Dr Neil Shearer for his expertise and support in generating electron micrographs.

Contents

Index of tables

Index of figures

1 Introduction

1.1 Project Aim

The aim of this study is to understand how the parameters of a nonwoven material govern Shielding Effectiveness (SE), in the microwave frequency range. There are a variety of factors, such as fibre length, metal coating thickness, caliper, porosity and more that may have a significant effect on the SE. Complicating this picture somewhat is the fact that many different SE analysis methods exist, all of which can produce different results.

1.2 Background

Electromagnetic interference (EMI) is an ever -increasing problem due to the sheer numbers of electronic applications that exist in today's world. There are many examples of systems that encounter EMI resulting in inadequate performance[1]. These include: mobile phones, electronic flight control systems, medical equipment, wireless networks, automotive electronics, and many more. For this reason many applications are housed in shielded environments.

EMI related effects typically don't manifest themselves into major problems for two main reasons. Firstly, over the last few decades electronic circuits and devices have been housed within metallic structures, which act naturally as electromagnetic shields. Secondly the typical field strengths associated with most everyday items are relatively small[A] and so a separation distance of few meters is often sufficient to minimise the effects of EMI.

However under-estimating the effects of EMI can lead to catastrophic failures as highlighted below.

- There have been multiple incidences of EMI influencing passenger aircraft's operation, including vast course and pitch change without instruction[2]. Often when the flight captains of such aircraft asked for passengers to check that all of their electronic devices (e.g. mobile phones) were turned off, the EMI related effects stopped immediately[3].

[A] See appendix 8.1 and Reference 15

- Five Blackhawk helicopters crashed shortly after their introduction in the 1980's. The causes of these crashes were all due to EMI between flight control systems and strong radar/radio transmitters[4].

- Early Harrier aircraft suffered catastrophic problems when landing vertically onboard aircraft carriers[5]. Cases of EMI radiating from the carriers radar equipment, and nearby sea vessels, triggered the aircrafts emergency ejector seat, killing the pilot.

- Trans World Airlines flight 800 exploded mid air killing all 230 people on board. No direct evidence as to why this disaster occurred was retrieved; however EMI and HIRF is believed to play a role[6].

More recently EMI has also been shown to cause more direct health issues associated with people living near strong emitters (such as mobile phone signal boosters and overhead power lines). There is no doubt amongst scientists that high intensity electromagnetic radiation emitted by phone masts can cause cancer and genetic damage[7].

In addition to this, cases of the extremely low frequency (ELF) radiation associated with overhead power lines have recently been re-categorised as "Possibly carcinogenic to humans" by the International Agency for Research on Cancer (IARC)[8].

1.3 Electromagnetic interference and composite structures

Many composite structures (from car wing mirrors to Nasa's space shuttles) are replacing traditional metallic structures in an effort to save weight. However this upgrade alone is not without penalty, often manifesting itself in the electrical properties of the structure. The conductive properties of composite materials are typically very poor compared to pure metals. This loss in conductivity often compromises the composite, especially when dealing with electromagnetic fields.

To compensate for this, a variety of highly conductive films, meshes and coatings have been developed to finish composite parts and boost their electronic performance. The

overall result is a composite structure that not only is much lighter than the original metal structure, but also just as conductive, allowing them to meet all of the application requirements (such as Electromagnetic Shielding) .
The nonwoven veils discussed in this report fit into this category of composite enhancing products.

1.4 Carbon fibre nonwoven materials

A nonwoven material can be defined as a web of fibres which has been bound together to form a porous sheet[9]. Traditionally, nonwovens have been synonymous with textile and fabric based materials. However in more recent times carbon fibre, and metal coated carbon fibre nonwoven materials have been developed, offering highly conductive, lightweight finishes. The figure below shows examples of woven and nonwoven carbon fibre materials. Nonwoven materials will be covered in more detail in section 3.2.

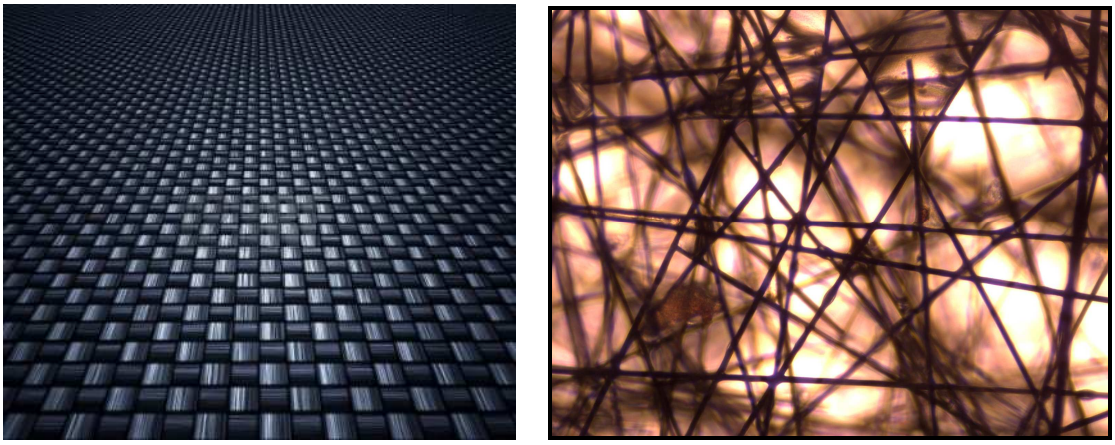

Figure 1: A comparison of woven *(left)* and nonwoven materials *(right)*. Nonwoven materials tend to be bound more by a polymeric compound rather than entanglement.

Nonwoven carbon fibre materials find applications in areas such as; Fuel cells, Lithium ion batteries, Wing de-icer elements, EM Shielding, Composite lightning strike protection and Radar signature management.

2 Literature Review

This literature review will discuss the current understanding in relation to four main areas. The four areas will follow a logical order, shown below:

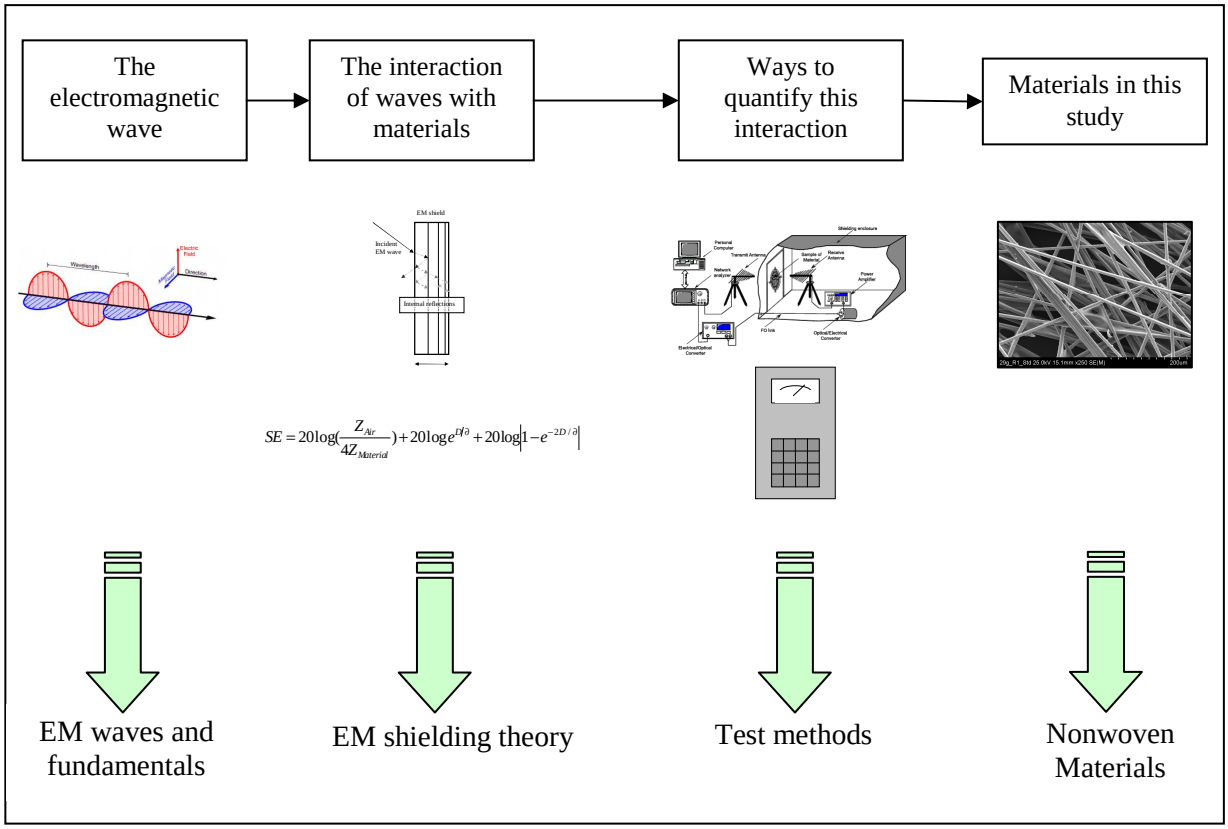

Figure 2: An overview of the literature review's content.

2.1 Electromagnetic waves

2.1.1 Fundamental principles

There are many examples of electromagnetic waves such as light, micro-waves, radio-waves, X-rays and many more. Such waves can be consolidated into an electromagnetic spectrum (figure 1), of many different wavelengths.

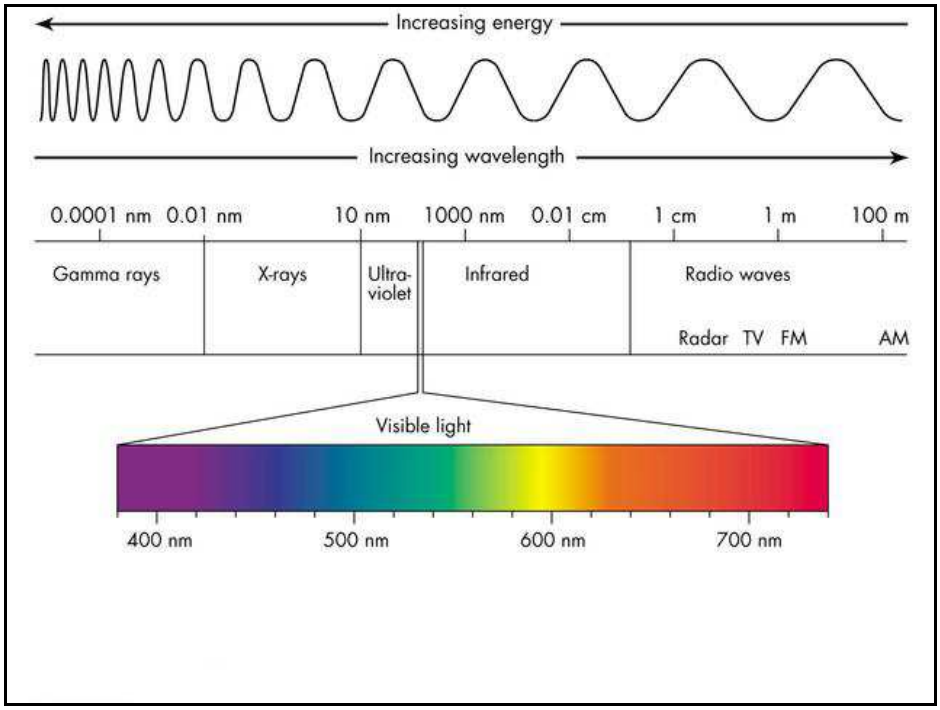

Figure 3: The Electromagnetic Spectrum[10].

Electromagnetic waves are transverse and consist of two fundamental components – an electric vector and a magnetic vector. One component cannot exist without the other. These two oscillating vectors are always generated perpendicular to one another and to the direction of wave propagation as represented below.

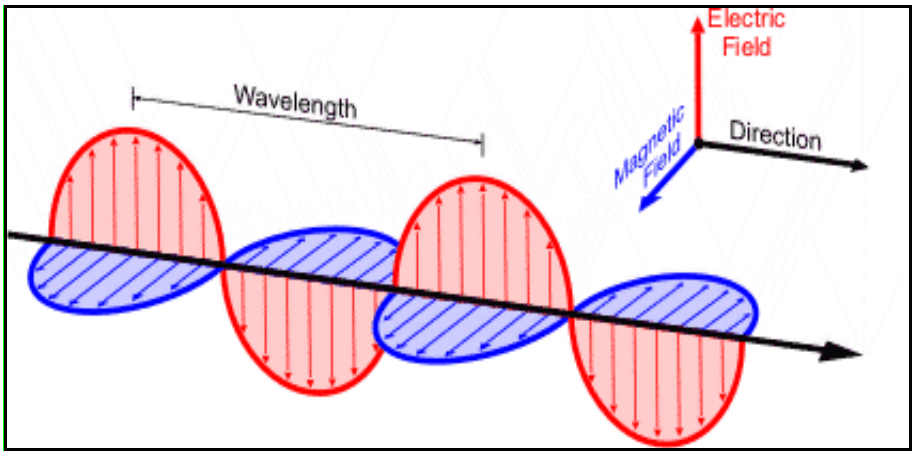

Figure 4: A Transverse Electromagnetic wave[11].

Electromagnetic waves are generated when a charge (e.g. an electron) undergoes non-zero acceleration. During this acceleration the moving charge radiates an oscillating magnetic field, which in turn generates an oscillating electric field.

This concept can be difficult to visualise but if we consider the opposite process in which an electromagnetic wave strikes an atom, it causes it to vibrate and undergo acceleration. It therefore makes sense that if we were to reverse time the opposite would be true (due to the time symmetry), and an Electromagnetic wave would be generated.

The electric and magnetic field components are coupled (figure 4) and propagate at the speed c (c = 3.00 x 10^8 m/s) in a vacuum. The speed of propagation is inextricably linked to frequency and wavelength by the relationship:

$c = f\lambda$ Where: f = *frequency* and λ = *wavelength*

And to reiterate:

1. An oscillating electric field $\hat{E}$ generates an oscillating magnetic field $\hat{H}$
2. An oscillating magnetic field $\hat{H}$ generates an oscillating electric field $\hat{E}$

A mathematical solution to this waveform can be expressed as:

$\hat{E} = \hat{x}E_0 \cos(k_z z - \omega t)$ for the electric component.

$\hat{H} = \hat{y}H_0 \cos(k_z z - \omega t)$ for the magnetic component.

Where:

$k = \frac{2\pi}{\lambda}$ =The wave number

E_0 = Amplitude of the electric field

H_0 =Amplitude of the magnetic field

$\omega = 2\pi f$ = Angular frequency

As is known, both the electric and magnetic fields oscillate in a sinusoidal manner an expression for the relative magnitude between these two components can be derived as the ratio E/H . This ratio is better known as the wave impedance Z (ohms).

2.1.2 Electromagnetic energy

All of the energy within an Electromagnetic (EM) wave is contained within the two electric and magnetic field components and as a result we can define the energy density using them:

The energy density in an electric field (U_e) is

$$U_e = \frac{1}{2}\varepsilon_0 E^2$$ Where: $E =$ Magnitude of Electric Field

$\varepsilon_0 =$ Permittivity of a Vacuum

The energy density in a magnetic field (U_h) is

$$U_h = \frac{1}{2}\frac{H^2}{\mu_0}$$ Where: $H =$ Magnitude of Magnetic Field

$\mu_0 =$ Permeability of a Vacuum

Therefore the total electromagnetic energy density can be expressed as

$$U = U_e + U_h$$

$$U = \frac{1}{2}\varepsilon_0 E^2 + \frac{1}{2}\frac{H^2}{\mu_0}$$

And as the known the energy associated with each field is equal:

$$\Rightarrow \quad E = cH \qquad \left(c = \frac{1}{\sqrt{\varepsilon_0 \mu_0}} \right)$$

2.1.3 Wave Propagation through a medium

The propagation of electromagnetic waves through any medium is governed by two parameters – the characteristic impedance z_0 and the propagation constant γ.

z_0 in free space is 377 ohms, however if the wave propagation was contained in a coaxial line cable (as is the case in later testing), z_0 is 50 ohms.

The propagation constant governs the wavelength and the attenuation of the wave moving through a medium. It is defined as:

$\gamma = \alpha + j\beta$ Where $\alpha =$ attenuation constant

$\beta =$ phase constant.

$$= 2\pi f \frac{\sqrt{\varepsilon_r \mu_r}}{c}$$

Hence we can define α and β as:

$$\alpha = \omega\left\{\mu\varepsilon'\left[\sqrt{1+\left(\frac{\varepsilon''}{\varepsilon'}\right)^2}-1\right]\right\}^{\frac{1}{2}} \qquad \beta = \omega\left\{\mu\varepsilon'\left[\sqrt{1+\left(\frac{\varepsilon''}{\varepsilon'}\right)^2}+1\right]\right\}^{\frac{1}{2}}$$

Where $\varepsilon' =$ real permittivity

$\varepsilon'' =$ imaginary permittivity

$$Tan\delta = \frac{\sigma}{\omega\varepsilon} = \frac{\varepsilon''}{\varepsilon'}$$

Consider $\frac{\varepsilon''}{\varepsilon'} = \frac{\sigma}{\omega\varepsilon}$:

For low loss (low conductivity) media $\sigma \approx 0$, $\alpha = 0$, and then $\gamma = j\beta$.

Hence we can set the following conditions:

$\frac{\varepsilon''}{\varepsilon'} \langle\langle 1$ Low-loss dielectric (low conductivity) material

$\frac{\varepsilon''}{\varepsilon'} \rangle\rangle 1$ Lossy (highly conductivity) material

2.1.4 Near and Far fields

When does the near field become the far field?

As an electromagnetic wave travels away from its source different behaviours dominate at different distances. Three separate boundaries can be defined: the near field (Fresnel), the far field (Fraunhofer) and the transition regions (as shown in figure 5).

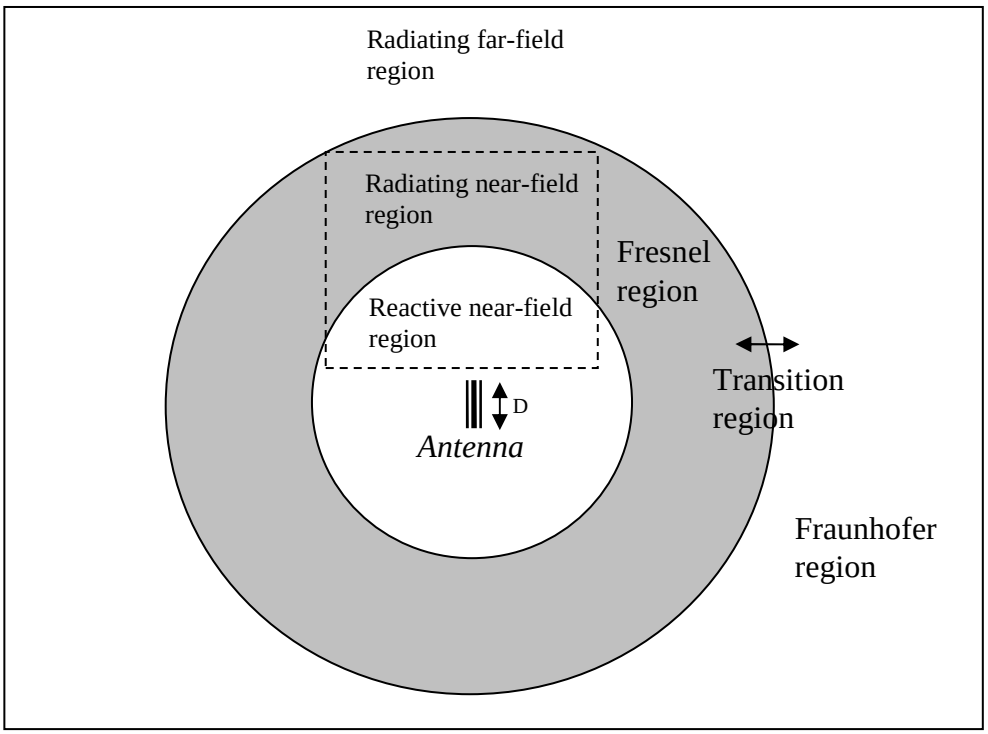

Figure 5: A waves behaviour as a function of distance from the source, can be defined by three different regions[12].

The Near Field

The near field region is split into 'reactive' and 'radiating' regions. Within this near field zone all polarisation types may exist (i.e. vertical, horizontal and circular).

At the (extremely close) ‘reactive nearfield zone’ the relationship between E and H field is very complex to predict and either E or H field may dominate. Therefore to calculate the power density at this point, separate measurements of E and H are required, as well as an additional phase relationship measurement between the two. This ‘reactive’ zone also has unknown amounts of energy stored close to the antenna’s surface which can lead to error in measurements. This is because the energy levels predicted by standard calculations (i.e the inverse square law) aren’t applicable at this close distance and so energy levels can rise more quickly than anticipated.

The remaining radiative zone contains no reactive components; however the relationship between E and H remains complex. The radiative zone occurs at a distance $0.62\left(\frac{D^3}{\lambda}\right)^{0.5}$.

The Transition Zone

The transition zone represents the distance between the near and far field and has characteristics of both. It is usually recommended that both E and H fields are measured in order to obtain a good approximation of the electromagnetic wave.

The Far Field

As the wave propagates further from its source, its impedance Z becomes a constant value of 377 ohms and the wave front can be accurately approximated as planar. The wave can be characterised by a single polarisation type vertical, horizontal or circular.

This far field point occurs at a distance approximately $\frac{2D^2}{\lambda}$ from the signal source, where ‘D’ represents the largest radiating dimension of the antenna.

Beyond this far field transition point the waves impendence remains at 377 ohms and does not change unless the wave interacts with a boundary of different impedance.

2.2 Shielding Effectiveness theory

The traditional methods for preventing the emission and/or reception of EM waves involve a range of strategies: from destructive interference techniques[13] to advanced material structures (such as radar absorbent materials (RAM) and EMI based faraday cages).

Background

Shielding Effectiveness refers to a materials ability to attenuate an initial EM signal and is measured in decibels (dB). Decibels are not a direct unit (such as Watts, Joules, Volts etc), but are used as they describe the ratio of one intensity measurement to another.

$$SE_e(dB) = 20\log\frac{E_I}{E_R}$$

SE_e = Shielding Effectiveness (E-field)
E_I = Strength of Incident wave (V/m)
E_R = Strength of Transmitted wave (V/m)

By replacing E_I, E_R with B_I, B_R the corresponding magnetic field can be calculated.

Due to the logarithmic nature of the dB scale it is important to realise that 20dB does not represent twice the Shielding Effectiveness as 10 dB.

Shielding Effectiveness (dB)	Signal attenuation (%)
10	90
20	99
30	99.9
40	99.99

Table 1: The relationship between SE and signal attenuation (as a function of power). 40 dB us equivalent to 99.99% of the signal power attenuation.

Therefore 40 dB represents a common threshold with regards to many application standards.

For the majority of this report positive values of SE will be used to represent higher levels of shielding. However in other texts and areas of this report negative notation is also used due to predefined software definitions.

The SE parameter can also be defined as the ratio of power received at the load with and without the test specimen in place, as shown below:

$$SE = 10\log\frac{P_0}{P_s}$$

Where P_0 is the power received at the load without the specimen, and P_s is the power received at the load with the specimen. As has already been defined, SE can be better understood by considering each mechanism in tern.

2.2.1 Current parameter and test method understanding

The following equations assume that the shielding material is both smooth, homogenous and a perfect conductor. This starting point will provide an equation, which can be later modified to accommodate nonwoven veil characteristics more accurately.

A materials plane will always reflect or absorb the energy from an EM wave. The degree of reflection and/or absorption can be expressed as the Shielding Effectiveness (*SE)* and is illustrated in figure 6.

$$SE = reflection(R) + absorption(A) + Internal\ reflection(IR)$$

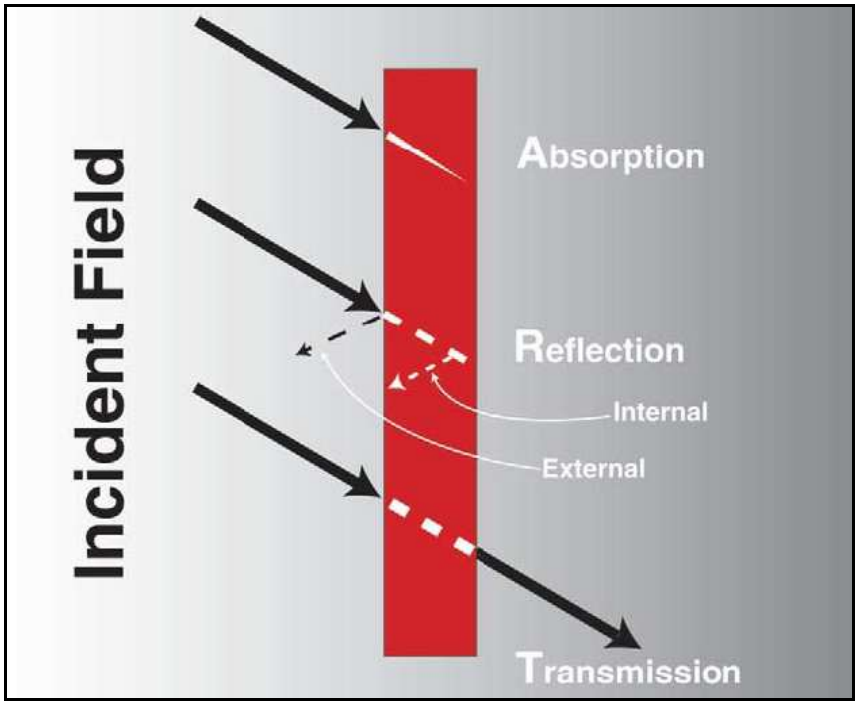

Figure 6: Shielding Effectiveness and the three mechanisms – reflection, absorption and internal reflection[14].

2.2.2 Reflection

If the mismatch between the impedance of the air and the impedance of the shielding material is large, then the greater the shielding by reflection.

$$R = 20\log\left(\frac{Z_{Air}}{4Z_{material}}\right)$$ Where: Z_{Air} = Impedance of air

$Z_{Material}$ = Impedance of the shielding material

For highly conductive materials Z can be expressed as:

$$Z_{Material} = \sqrt{\frac{\omega\mu}{\sigma}}$$

$\sigma = Conductivity$

$\omega = 2\pi f$ Where f = frequency

$\mu =$ *Magnetic Permeability*

However for materials that exhibit low levels of conductivity the impedance must be expressed as:

$$Z_{Material} = \sqrt{\frac{\mu}{\varepsilon - j\frac{\sigma}{\omega}}}$$

$\varepsilon =$ Electric permittivity

Typically electric fields are high in impedance, which results in a mismatch with a low impedance (or high conductance) shield. Therefore high levels of reflected attenuation would be seen.

Magnetic fields are low impedance, which matches the shielding material.
Therefore limited reflected attenuation would be seen.

2.2.3 Absorption

Absorption *(A)* occurs as the EM field attempts to pass through the shielding material and is dependant on the

1.Electrical conductivity of the shielding material
2.Magnetic permeability of the shielding material

The resulting attenuation is exponential and quantified by skin depth (∂). Skin depth is defined as the distance an EM wave travels into a shield until only 37% of its original power remains.

$$A = 20\log e^{\frac{D}{\partial}}$$

Where: $$\partial = \sqrt{\frac{1}{\pi f \mu \sigma}}$$

D = Thickness of shield

Absorption is the dominant mechanism of shielding when electrical conductivity and magnetic permeability of the shield are high.

2.2.4 Total Shielding Effectiveness

Substituting the expressions of *R and A* into the below expression:

$$SE = reflection(R) + absorption(A) + Internal\ reflection\ (IR)$$

We find:

$$SE = 20\log(\frac{Z_{Air}}{4Z_{Material}}) + 20\log e^{D/\partial} + 20\log\left|1 - e^{-2D/\partial}\right|$$

The first term describes the reflection loss, the second term the absorption loss and the final term any internal reflection loss. Internal reflections occur when an EM wave

penetrates into the bulk of a material and is then re-radiated/scattered by internal structures within the shield, as illustrated in figure 7.

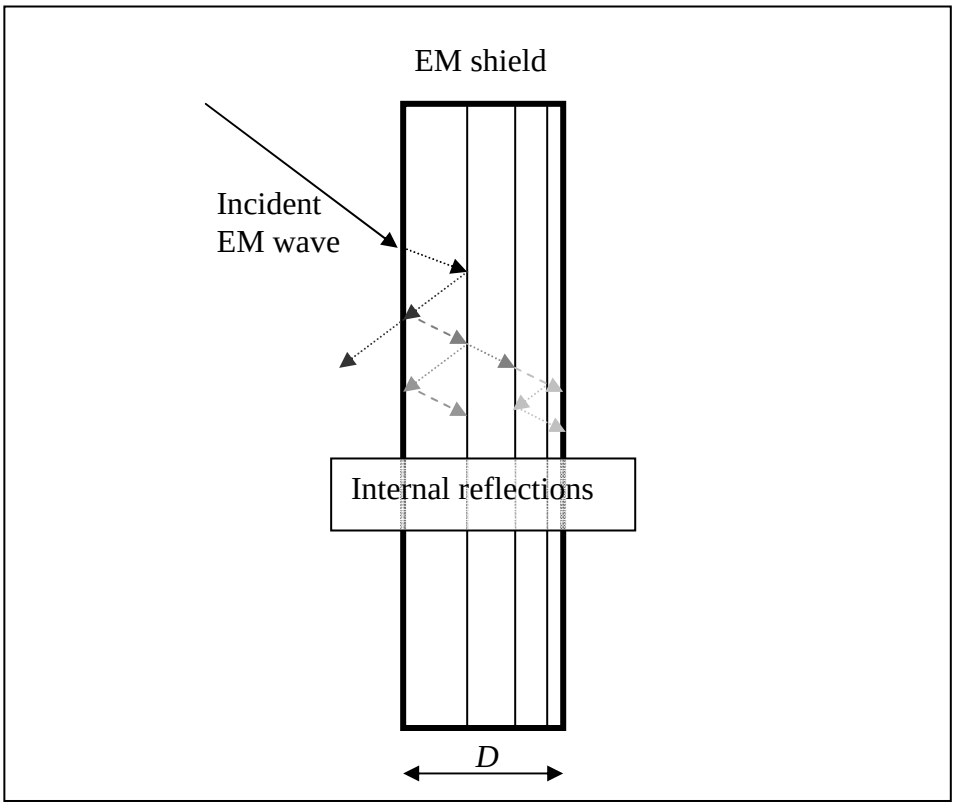

Figure 7: A demonstration of the shielding mechanism Internal Reflection. The vertical lines within the shield represent idealised internal structures in which the incident EM wave can interact.

It is important to realise that the internal reflection loss term need only be considered when the distance *D* is large compared to the skin depth ∂.

2.3 A review of Shielding Effectiveness Test methods

Current test method standards

The theory above is well accepted and understood. However problems often arise putting this theory into practise. Design of a valid SE experiment is difficult because there are many external factors that contribute to the result obtained: sample size, sample shape, the geometry of the test setup, and the source of EM radiation.

Further to this many of the established, legitimised measurement standards have limitations, which have lead to unrestrained modifications and practises. For these reasons no industry wide test consensus exists.

Despite the lack of a unified test method, many test standards and regulations have been written. They often specify particular test methods for different EMI related products e.g. conductive gaskets, paints, coatings, films, plastics and enclosures. Some of these can be seen below:

Enclosures and planar materials

- MIL-STD 285 – Shelters - *Withdrawn*
- ASTM E1851 – Shelters (duplicates MIL-STD 285)
- IEEE STD 299 – Shelters (replaced MIL-STD 285)
- ASTM D 4935 – Planar Materials - *Withdrawn*
- Reverberation Chamber Tests, TEM Cells
- NSA 65-6, 73-2A, 94-106 – Tempest Shelters
- SCTE 48-1-2006 – GTEM Cell Tests
- EN 50147-1 – Anechoic Chambers
- IEC 61000-5-7 - Enclosures
- VG 95373 Part 15 – Small Enclosures

Gaskets

- IEEE STD 1302 – Guide to EMI Gasket Test Methods
- SAE ARP 1705 – EMI Gasket Transfer Impedance
- SAE ARP 1173 – EMI Gasket Radiated Field

– MIL-DTL 83528 – Conductive Elastomer EMI Gasket Radiated Field and DC Volume Resistivity

As gasket based shielding technology is less relevant to the current development area, this report will focus on enclosure and planar types of test method.

2.3.1 MIL-STD-285 & IEEE 299-1991/2005

The most well known shielding standard is MIL-STD-285 introduced in 1956. It describes a radiated field test in which the signal source is placed outside an enclosure and the receiving device is located inside. The latest version of this standard covers frequencies from 100 KHz - 10 GHz and can be see in figure 8 and 9.

When testing a material for its shielding properties, it is important to design an experiment that mimics the application as closely as possible. For instance designing a material to exclude incoming RF waves (i.e maximum reflection loss), the transmit antenna should always be placed outside the enclosure.

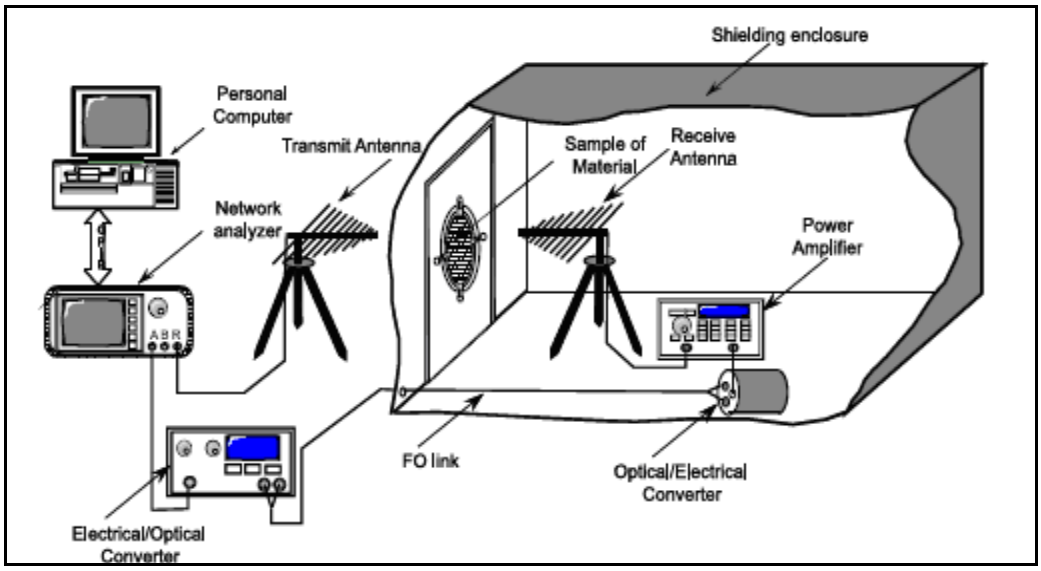

Figure 8: An adaptation of the MIL-STD-285 method. This setup would be used for enclosures designed to exclude RF emission from external sources[15].

However when trying to design an enclosure for the containment of RF waves, maximum absorbance loss is desired (to prevent self interference). Then the transmitting and receiving antenna should be swapped, such that the transmitting antenna is inside the enclosure – mimicking the application.

Figure 9: ***(Left)*** **The MIL STD-285 method: The transmitting horn and material under test are seen.** ***(Right)*** **The image shows the shielded room in which the whole test setup is within. The walls are clad in a copper alloy lining and EMI gaskets have been applied to the door to prevent any external interference from affecting the results.**

This standard was later replaced by IEEE STD 299-1991 which extended the frequency range to 50 Hz – 100GHz. IEEE STD 299 – 2005 has since updated the 1991 standard by providing values of uncertainty within EM measurements. Despite these adaptations, the latest standard is still regarded as a derivative of the original concept.

2.3.2 ASTM D4935 (Near field)

The American Society for Testing and Materials (ASTM) has developed several SE standards. In 1989, ASTM developed D4935, which enabled the SE of planar materials to be determined over 30 MHz to 1.5 GHz. This was revised in 1999 to include the scope of applications that the method can be applied to. Further details of the ASTM method can be seen in figure 10.

Electromagnetic waves are generated by the network analyser and transmitted across the flanged coaxial waveguide. Test samples are placed between the waveguides and the shielding effectiveness can then be then inferred.

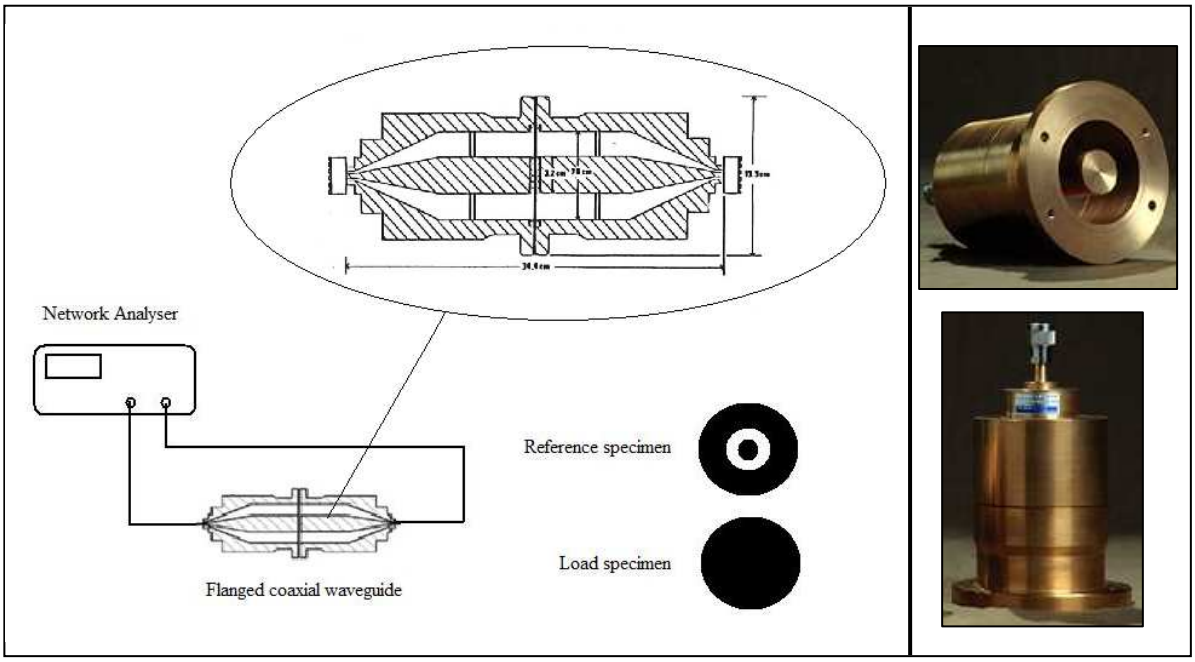

Figure 10: A schematic diagram detailing the ASTM D4935 test method. The images on the right shows the flanged coaxial waveguides split into two pieces.

However in 2005 the committee ASTM D09.12 withdrew the standard as they lacked the technical expertise to maintain it. There are also concerns regarding reflections and grounding of the materials under test, which could lead to inaccuracies.

The information within this standard is still widely used to determine the SE of planar materials.

2.3.3 Waveguide Transmission Line (as used in this study)

This method is based on the same theory as the ASTM D4935 standard above. The method replaces the large coaxial waveguides in *figure 10* (*right*) with rectangular waveguide horns. The waveguides are connected to a network analyser via a 50 ohm coaxial cable. They are then connected at their flat edges allowing for a measurement range between 1 – 100 GHz (provided different waveguides are possible).

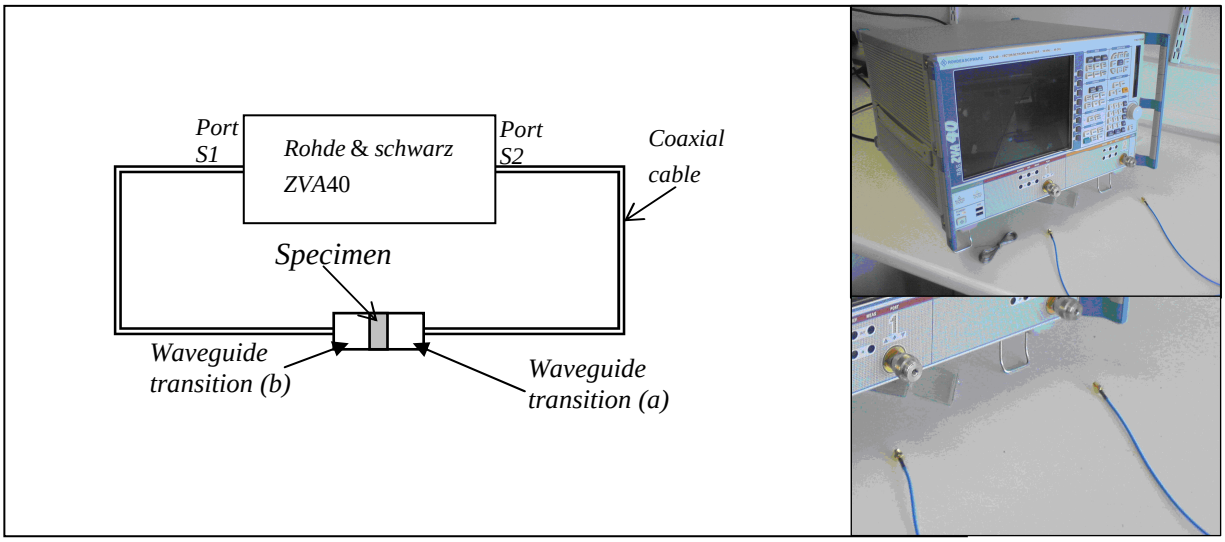

Figure 11: A simple schematic of the near field test method; photographs portray the network analyser and coaxial cables.

Further details of this test setup will be provided in the experimental aspect of this report (chapter 4). The test method is relatively efficient to perform (compared for example to stirred mode chamber testing) and allows S-parameter data to be obtained quickly.

The main difficulties with this type of test setup are:

- Alignment of the waveguide-sample-waveguide interface is crucial, but difficult to obtain, particularly if precision waveguide dowels are not fitted.
- Electrically thin samples may only be tested as the accuracy of the test setup falls dramatically when the waveguides are separated by any significant distance [B].
- Any reflections from the sample, can generate a standing wave leading to resonant effects and unwanted noise in the results[C].

[B] Design of a valid test cell can allow for thicker samples (even liquids) to be tested.
[C] Advanced 'TRL' calibration methods help this effect but do not entirely remove it.

- Any air gaps between the sample and the waveguide walls will ‘dilute’ any measurements of the sample permittivity.

2.3.4 Far field testing (Redheffer)

The free space, far field equivalent of this test method is still being developed at Napier University. The concept makes use of a pair of spot – focusing horn lens antennas, mode transitions, coaxial cables and a Network analyser (as shown in figure 12).

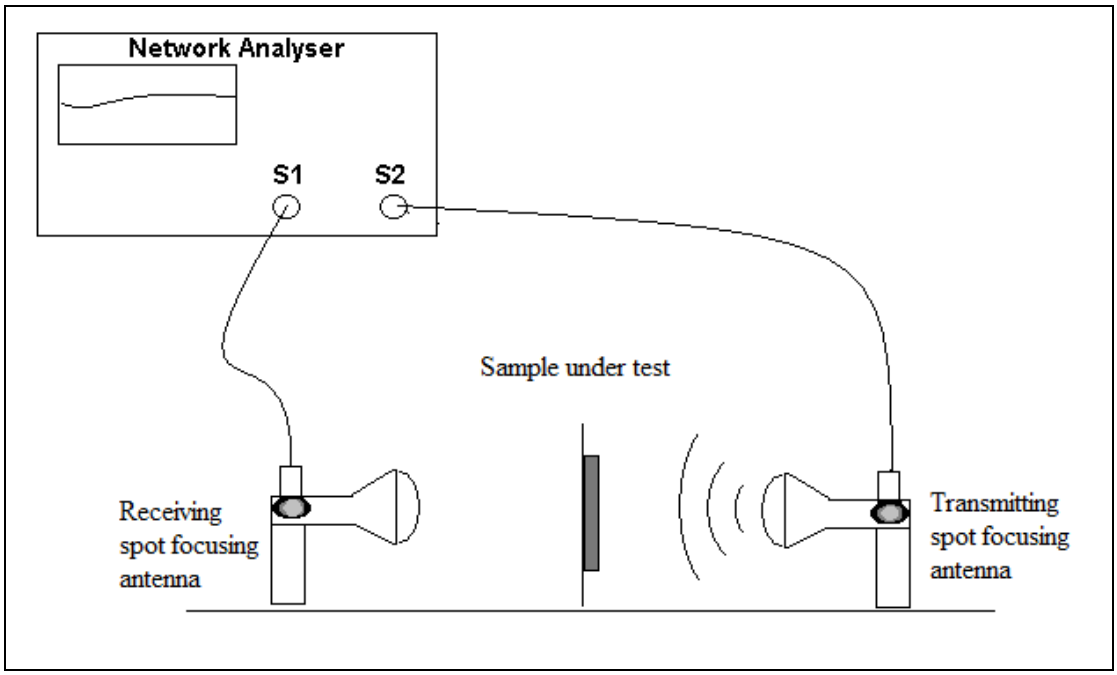

Figure 12: A simple schematic of the ‘Redheffer’ far field test setup.

The main errors associated with this type of test setup involve

i) ‘Diffraction effects’ around the edge of the sample
ii) Multiple reflections between the lens antenna and mode transitions

However a plano-convex focusing lens can be used to minimise the diffraction effects from the sample and its surroundings and, time domain gating (a feature of the network analyser) can be used to correct for reflective and transmissive errors arising from multiple reflections.

Through, Reflect and Line (TRL) calibrations can also be used to remove multiple reflections effectively.

2.3.5 Stirred Mode Reverberation Chambers (SMRC)

An SMRC is a shielded room in which an EM field is generated and stirred using a metallic paddle. The paddle is designed to vary the boundary conditions of the chamber and hence create the entire mode conditions present in a statistically uniform field.

Stirred mode chambers replaced the more commonly used shielding methods such as the MIL-STD-285 (which often suffer from repeatability and precision).

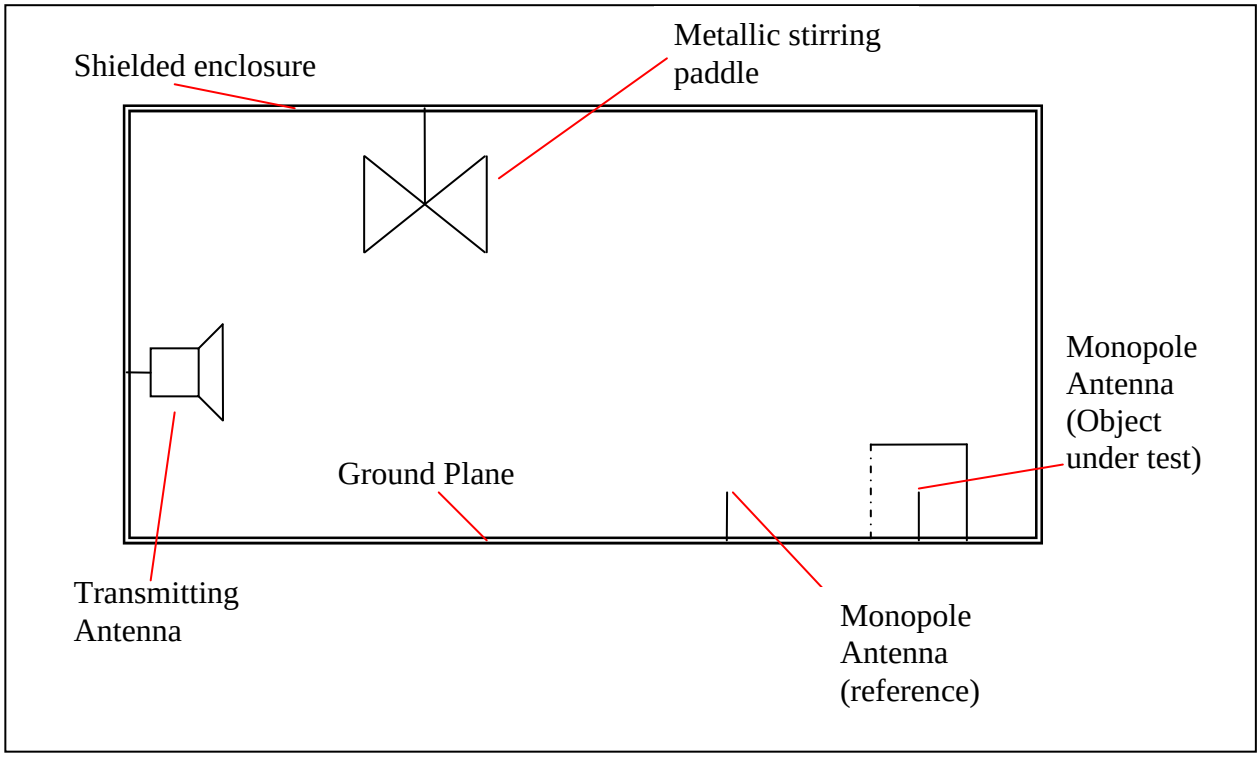

Figure 13: A schematic of an SMRC.

Mechanical stirring of the field modes can be replaced by frequency stirring. This involves either sweeping the source over a particular bandwidth or frequency modulating the signal that is projected into the chamber. Distinct frequency peaks are created that are replicated within the 'object under test'. The shielding properties of the object under test can then be deduced by measuring the reduction in amplitude of these peaks.

To ensure that the field within the chamber is indeed uniform, there must be at least 60 modes present. To achieve this, the quality factor of the chamber must be high. A longer wavelength (or smaller chamber) results in a decreased quality factor. This derives a low frequency condition – below which quasi-static fields are created. Such conditions create non-uniform field strengths at different points within the chamber, making testing less accurate.

Typical testing frequencies are 10 kHz – 100 GHz. The disadvantages to SMRC methods are associated with the processing times it takes to analyse a particular sample. Depending on the sample bandwidth, testing of a single specimen can last from an hour up to a day.

2.3.6 Quasi-optical free space focused Gaussian beam method

Rather than to try and correct for the errors associated with the Redheffer far field setup, this method removes them altogether. This is achieved by changing the geometry of the test setup and by generating EM waves from corrugated horns, with a Gaussian profile.

Gaussian beams are advantageous as they are:

- Fully calculable along their length.
- Can be focussed by concave mirrors.
- The outer regions of the propagating ray decays exponentially into negligible amplitudes.

These features effectively remove the diffraction problems often encounted in free space shielding measurements.

The geometry of this quasi-optical method can be seen below.

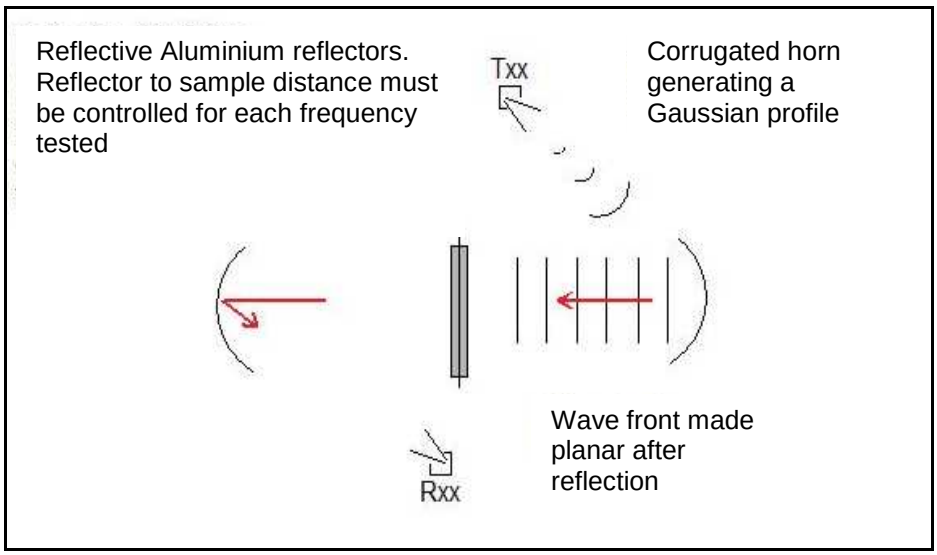

Figure 14: A schematic of an alternative free space measurement using the 'quasi-optical free space focused Gaussian beam method'

As the testing frequency increases, the focusing of the Gaussian beam can be achieved to higher levels. Further to the geometric changes and wave profile – time domain gating can also be used to improve the accuracy of this setup.

The main disadvantages of this type of setup involve:

- Tight tolerances on the geometrical setup and calibration of the horns, mirrors and sample.
- The large physical dimensions of the test setup mean that the samples sizes also need to be much bigger, compared to waveguide techniques.

2.4 Nonwovens and similar materials

The nonwoven veil has a diverse range of parameters all of which will impact on its ability to shield EM waves. These parameters include;

Fibre length	Thickness (Caliper)
Fibre orientation	Formation quality
Metal coating thickness	Fibre diameter
Coating type	Binder systems
Density	Particulate addition

Table 2: A listing of the parameters thought to influence the electrical properties of the nonwoven veil.

It would be ambitious to try and quantify all of these factors within the timescales of this report. Therefore this report will focus on; Fibre length, Metal coating thickness, Metal coating type, and Formation quality.

The stochastic matrix structure of the veil (figure 15) makes parameterisation challenging and often couples parameters together (for example veil polarisation via fibre alignment often impacts on the veils thickness and density.

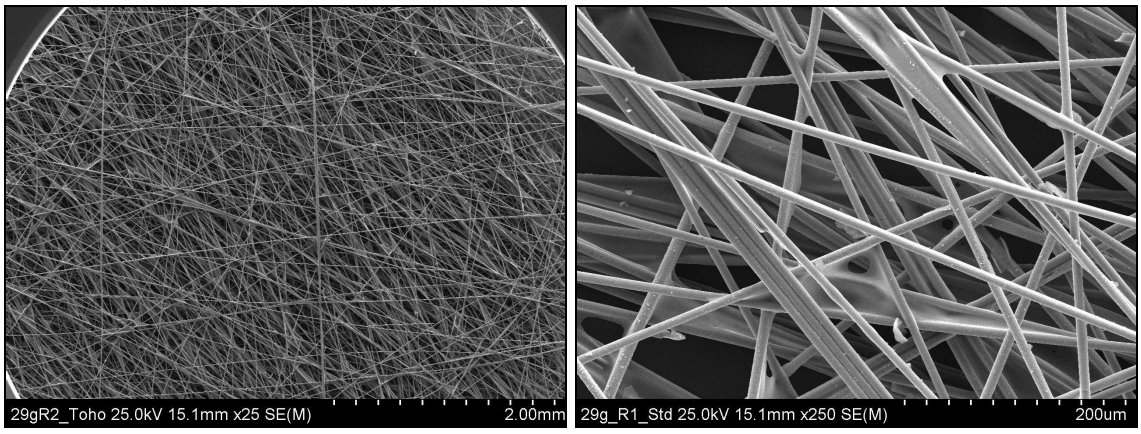

Figure 15: A matrix web of fibres forming a carbon fibre nonwoven veil.

3 Experimental

The previous section discussed a range of SE test setups that are used throughout the microwave industry. This section concentrates on the particular test setup used in this study.

3.1 Introduction

In order to generate a broad range of results, a variety of techniques were used including:

- Shielding Effectiveness measurements
- Resistivity testing (DC)
- Thickness and basis weight determination
- Scanning Electron Microscopy (SEM)
- Energy-dispersive X-ray spectroscopy (EDS)

These analysis methods will now be discussed in more detail.

All of the materials discussed and analysed in the following sections were coated at Electro-Fiber Technologies (EFT) and manufactured into veils at Technical Fibre Products (TFP). Some studies took more than one trial to complete, in which cases dispersion characteristics and machine settings were kept the same. This ensured consistent processing conditions which made for confident analysis.

3.2 SE test Method

A Rohde & Schwarz network analyzer (ZVA40) was used to probe the scattering (S) parameters associated with the reflection, absorption and transmission of EM waves by different shielding media. These parameters were used to obtain the total amount of shielding attenuation provided at 4 main frequency ranges 2.6 – 3.95GHz (S-band), 8.2 – 12.4GHz (X-band), 15 – 22 GHz (K-band) and 25 – 40GHz (Q-band).

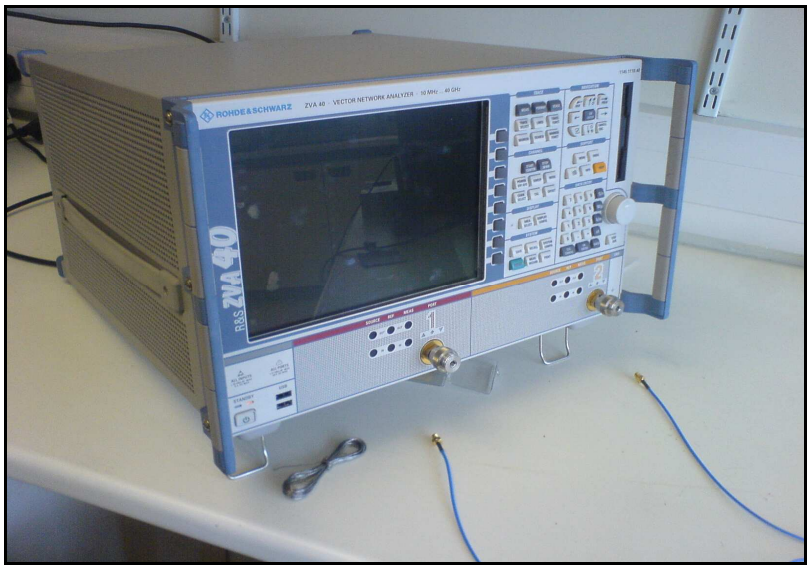

Figure 16: An image of the Rohde and Schwarz Network Analyser.

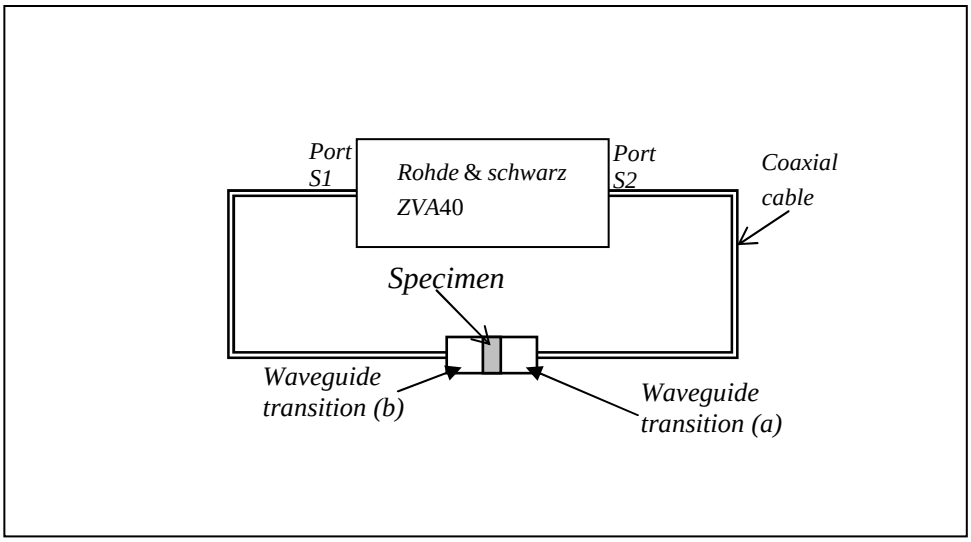

Figure 17: A simple circuit diagram of the test setup.

To carry out a measurement of SE, the specimen is first secured between the two waveguide transitions. A signal is then generated from port ‘S2’, which propagates through the coaxial cable, waveguide transitions and specimen and arrives at port ‘S1’ a short time later.

As the propagating wave meets the material under test, the wave is reflected, absorbed or transmitted. The extent to which each interaction mechanism contributes to the total SE loss is dependant on the material properties of the specimen such as conductivity, permeability, permittivity, thickness etc. Reflective measurements can be characterised by

selecting the network analyser to read ‘S11’ or ‘S22’ port data. Similarly transmission measurements are achieved by selecting ports ‘S21’ or ‘S12’.

The network analyser was setup to generate a higher order transmission line using the dominant TE_{10} mode. This differs from standard transverse EM lines due to the fact that at least one significant field component is aligned with the direction of propagation. Rectangular wave guide flanges were used to achieve this.

Figure 18: ***(Left)*** **X-band waveguide transition, *(Right)* S-band waveguide transition.**

The samples to be tested were cut to the relevant waveguide size, such that their dimensions exceeded the waveguide aperture sizes below.

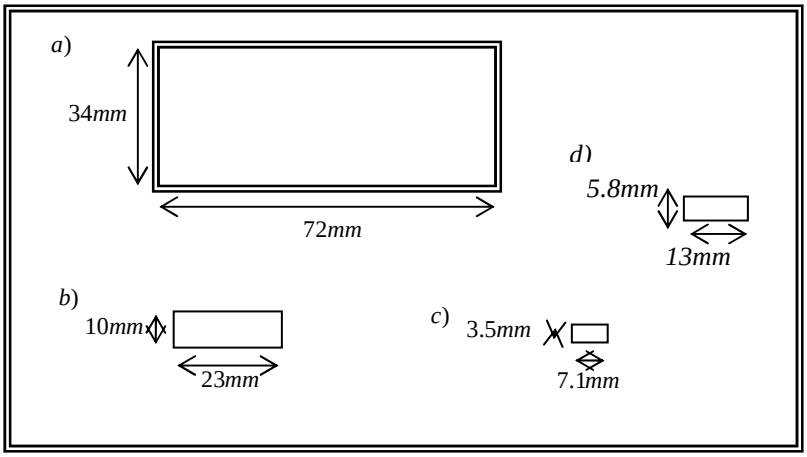

Figure 19. The physical dimensions of the aperture of each wave guide used.

a) S-band waveguide aperture (WG10)

b) X-band waveguide aperture (WG 16)

c) Q-band waveguide aperture (WG22)

d) K-band waveguide aperture (WG 19).

3.3 Network Analyser Calibration

The Network Analyser allows for a wide range of calibration methods for different types of measurement.

The method used in this experiment was a simple 'through' calibration. This allowed normalisation of the setup, which compensates for frequency dependant attenuation and phase shifts in the signal path.

A more advanced TRL (Through, Reflect, Line) calibration method was identified which helped remove some of the signal noise recorded in the results. Future work will incorporate this more advanced calibration method.

For a guide to the calibration method please see appendix 7.2.

3.4 Sample preparation method

A specimen from each sample was first cut to the correct size, depending on the frequency band to be tested. For repeatable results that could be averaged, 3 specimens of each sample were cut in the Machine direction (MD) & cross direction[D] (CD).

This must be repeated for each frequency band.

	MD	CD
Q-band = 7.11mm x 3.55mm	x3	x3
X-band = 23mm x 10mm	x3	x3
K-band = 5.8mm x 13mm	x3	x3
S-band = 72mm x 34mm	x3	x3

*These are the dimensions of the waveguide aperture itself. The sample templates seen in **figure 18** are slightly bigger than these sizes to enable ease of alignment. Also for square specimens, only one direction of cutting is needed, as the sample can be rotated 90 degrees to simulate either MD or CD directions.*

[D] The Machine direction (MD) refers to the direction in which the material was manufactured. 90 degrees to this is the Cross direction (CD). Naturally the fibres tend to align themselves (slightly) in the MD.

1. Each sample is placed between the waveguides, which are held together using the Vice at ‘hand tight’ pressure. Make sure that the sample is aligned perfectly with the waveguide.

2. Then navigate to ‘File’ $\Rightarrow$ ’Trace Data’ $\Rightarrow$ ’Export Data’. Name the data appropriately (i.e. specify the grammage, material, frequency band and whether the measurement was MD or CD) and store it as a ‘.csv’ file.

   It important to ensure that the power band average is set to 1 kHz. This sets the sampling frequency to 200 measurements per sample are recorded.

3. This should be repeated 3 times in the MD direction and 3 times in the CD direction before moving onto the next sample or frequency range.

4. To recall the data, open the Excel ‘.csv’ file. The data will be separated by a comma (**csv** = comma separated value). See appendix 8.3 for further details.

   A) Select column ‘A’ of the spreadsheet so that all the values are highlighted. The click on the ‘Data’ tab at the top of the Excel spreadsheet

   $\Rightarrow$ Text to column

   B) $\Rightarrow$ Select ‘delimited’ and then ‘next’

   C) $\Rightarrow$ In the ‘delimiters’ section then check the semicolon box.

   D) $\Rightarrow$ Then click finish.

   The data should now be presented in two separate columns.

3.5 Surface resistance (DC) method

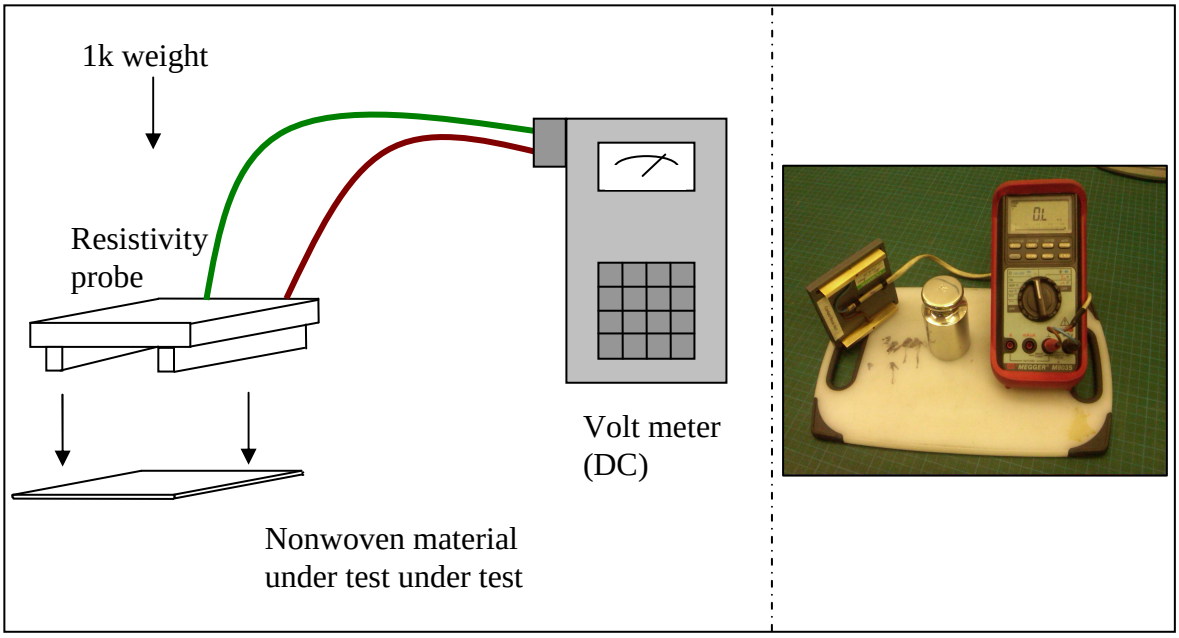

Figure 20: A sketch and photograph of the surface resistance test method used.

As all of the materials are thin (typically ~ 200 microns), an assumption has been made that surface resistivity results can be used to approximate the bulk resistivity.

This two wire test method is first calibrated such that any resistance in the cables is corrected for. A sample of the nonwoven to be tested is then cut to $10\,cm^2$ and placed underneath the probe. A 1kg weight is placed onto of the probe to provide a consistent pressure whilst a recording of the resistance is taken.

To check for sample anisotropy the sample is then orientated through 90 degrees and a further measurement taken. Additionally the bottom side of the test sample is also characterised to check for any polar manufacturing defects. A minimum of 5 samples were characterised and the results averaged in order to provide repeatability and standard deviation.

An example of surface resistivity results is shown in section 4.2.

3.6 Scanning Electron Microscope (SEM) methods

Scanning electron micrographs

In various parts of this report electron micrographs of the nonwoven materials have been generated in order to gain a better understanding of the nonwoven's fine structure. This technique was particularly useful when analysing the distribution of particles within a nonwoven structure (as in *section 4.5*). Other qualitative factors such as the average number of fibre to fibre (node) contacts could also be established.

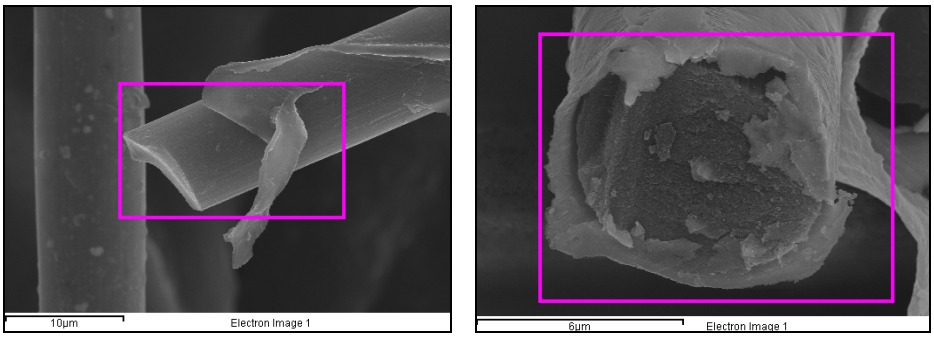

Figure 21: (*left)* A scanning electron micrograph of a damaged carbon fibre
(*right*) A scanning electron micrograph of a copper coated carbon fibre

Energy-dispersive X-ray spectroscopy (EDS)

As a more quantitative method (c.f micrographs alone), EDS enables detailed elemental analysis and mapping of the nonwoven structure. This analysis method was important as it proved whether or not nonwovens were free from contamination, oxidation and reaction.

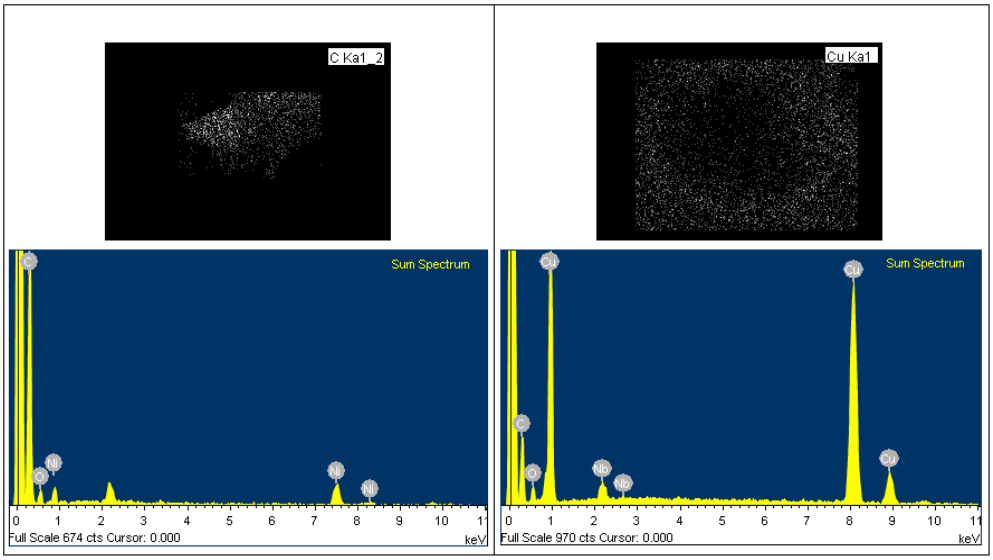

Figure 22: (*Top left) EDS* X-Ray mapping of carbon in figure 18 (*left)*.
(*Top right)* EDS X-Ray mapping of copper figure 18 *(right)* .
(*Bottom left)* EDS X-Ray elemental analysis of carbon fibre
(*Bottom right)* EDS X-Ray elemental analysis of a copper coated carbon fibre

3.7 Optical scanning analysis methods

HP Scanner TWAIN 3800 – Image Analysis

The manufacture of any product always has a degree of variability, and the same rule applies for the nonwoven materials that are considered in this study. The main contributing factor to this variability is the formation quality of the fibres. A 'poorly' formed material typically has much lower performance parameters compared to a material that has been formed 'correctly'. A 'poorly formed material' is one with an uneven distribution of fibres and fibrous clumps across its area. A 'correctly formed material' has a much more even distribution and is does not contain any fibre clumps.

Any variability is minimised by keeping the machine processing conditions exactly the same. However due to the stochastic nature of the manufacturing process, some sample variability will always be present, and an analysis of this is required before any cross comparisons between sample sets are made. Optical scanning analysis was the method chosen to do this.

The formation of a sample is analysed by retrieving a high resolution image of the desired sample. The scanners slide input function (Transparent Media adapter [TMA]) is activated so that the analysed image represents a measure of the samples true formation and not just a surface image scan. The image is then scanned as a greyscale and pixelated. The pixilation generates a spectrum of different grey shades that can be averaged to represent an area of the image (as below).

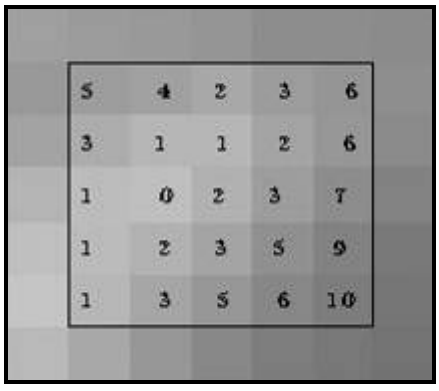

Figure 23: Grey shades are generated based on the scanned characteristics of a nonwoven sample. This allows the formation quality of the nonwoven to be analysed quantitatively.

This image is then filtered using a posterisation process - decreasing the amount of grey shades and simplifying the data to be analysed. A histogram is then used to plot the percentage of pixels that exist against of a certain grey shade (defined by a number).

Once plotted a graph similar to the examples shown in figure 24 can be generated.

An interpretation of the likely graph formations are also defined in each histogram. A sharper Gaussian peak represents a better formation of fibre as a smaller range of grey scales is evident. This peak shifts to the left for heavier basis weight material as darker grey scale values are present due to the reduction in transmitted light at the scanning stage.

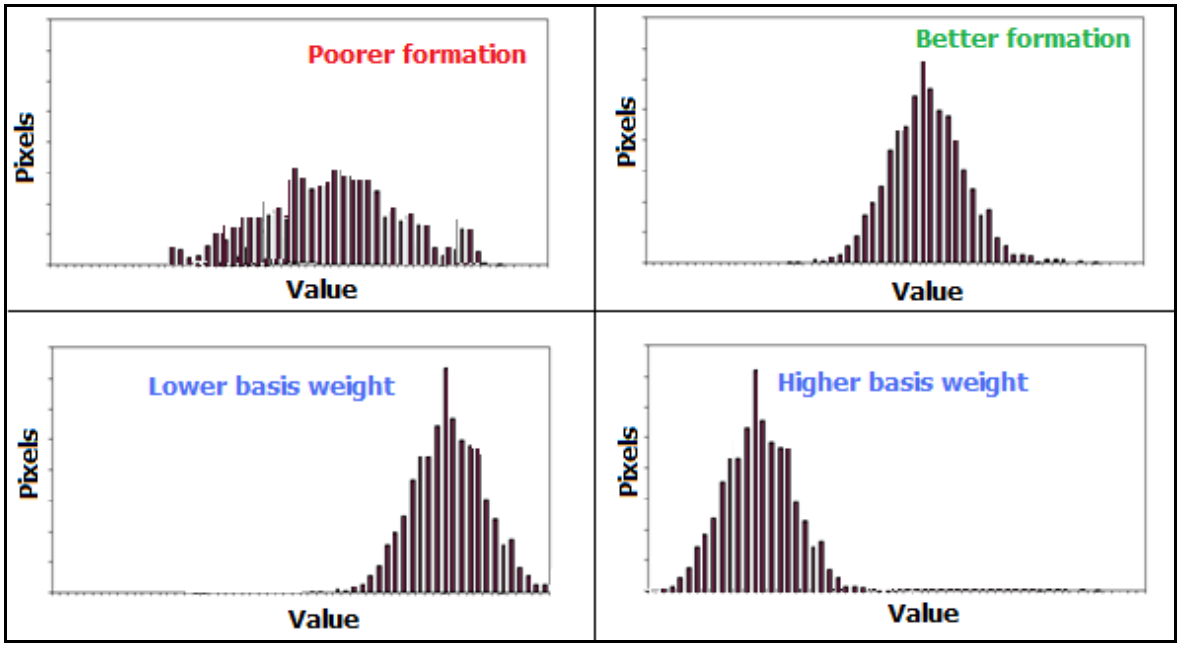

Figure 24: The interpretation of different trends that are obtained for samples with different formation properties and characteristics.

By ensuring that the formation quality of different samples is similar – one can confidently make comparisons based on intrinsic material differences rather than those that are based on variability.

4 Results and Discussion

4.1 Effects of changing the basis weight

The main aim of this experiment was to understand how the basis weight of a carbon fibre veil influenced the total transmission loss (S21) and hence generate SE data.

4.1.1 Introduction

The carbon fibre veil is the simplest material considered in this report as there is the least amount of variables or components that may skew or impact on the results. Therefore it is the best candidate to test the hypothesis: how does SE vary with basis weight?

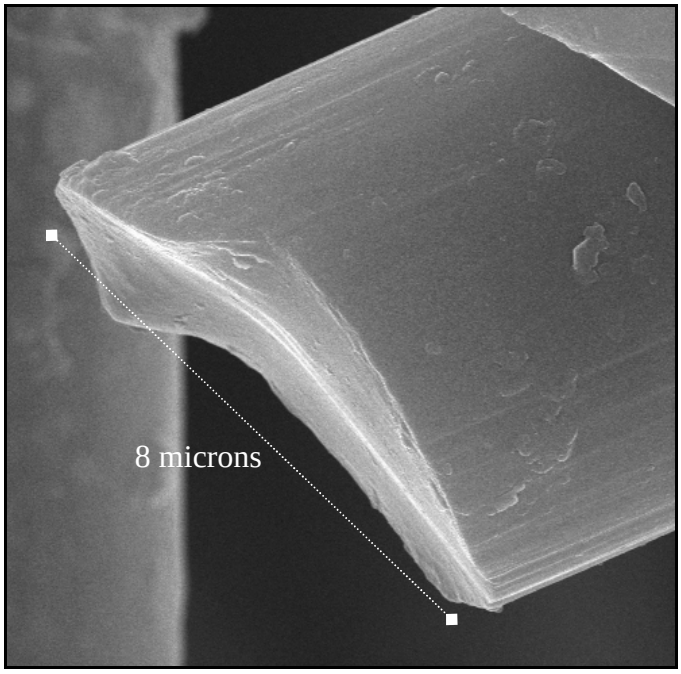

Figure 25: An SEM image of single fibre used construct the matrix that makes up the carbon fibre nonwoven veil.

The specific grade of carbon fibre used is Polyacrylonitrile (PAN) which is formed by extruding and processing an acrylonitrile-based polymer. This is the same variety of carbon used in this study. At later points within the report (sections 4.2 onwards), PAN carbon forms the core fibre which is then coated in a variety of metals.

4.1.2 Results and discussion

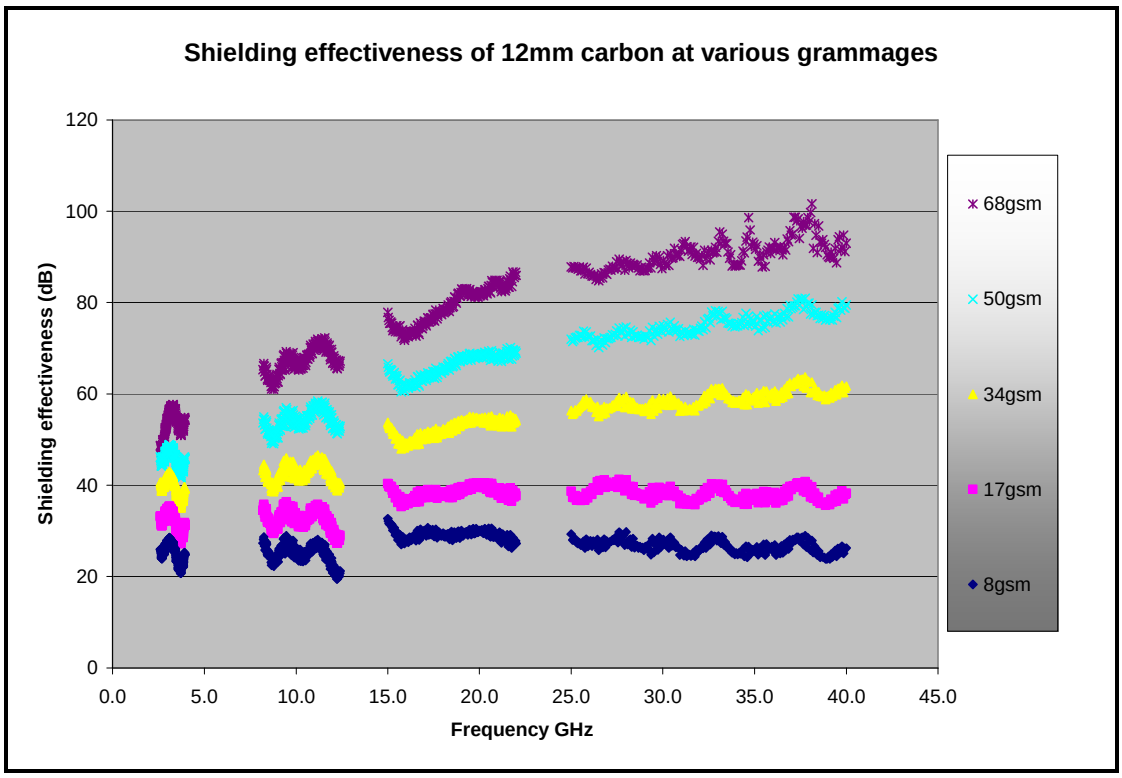

Figure 26: The Shielding Effectiveness of carbon fibre nonwovens at different basis weight (or grammage).

There is a direct relationship between the basis weight of the material and the SE obtained. It can be clearly seen that heavier materials shield more effectively than lighter materials at all frequencies. Each shielding response also demonstrates frequency specific trends resulting in higher levels of shielding at higher frequencies. This effect is greater for materials that are 34gsm and above.

Increasing the basis weight results in greater SE for two main reasons: a) The heavier basis weights have more fibres per unit area. This reduces the average pore size of the material allowing it to approximate the surface of an unbroken film more effectively. b) The heavier basis weights are more conductive and so there is a greater mismatch in the reflection term of SE equation. The result is more reflective loss and hence more overall shielding.

Skin depth

Skin depth is a measure of how deep electrical conduction may take place within a material. As an EM wave interacts with a conductive material, it causes an alternating current to flow within that material. This AC current flow is greatest at the materials surface and falls as a negative exponential (e^{-1}) as one approaches the materials core.

This is not true of DC currents, as the whole cross sectional area of the conductor is used to pass current.

Although the magnetic permeability has not been measured experimentally, for non-ferromagnetic materials (such as carbon fibre) it can be assumed that its value is equal or close to 1 at all frequencies. Values of conductivity were obtained, allowing for the following graph of skin depth's Vs frequency to be plotted.

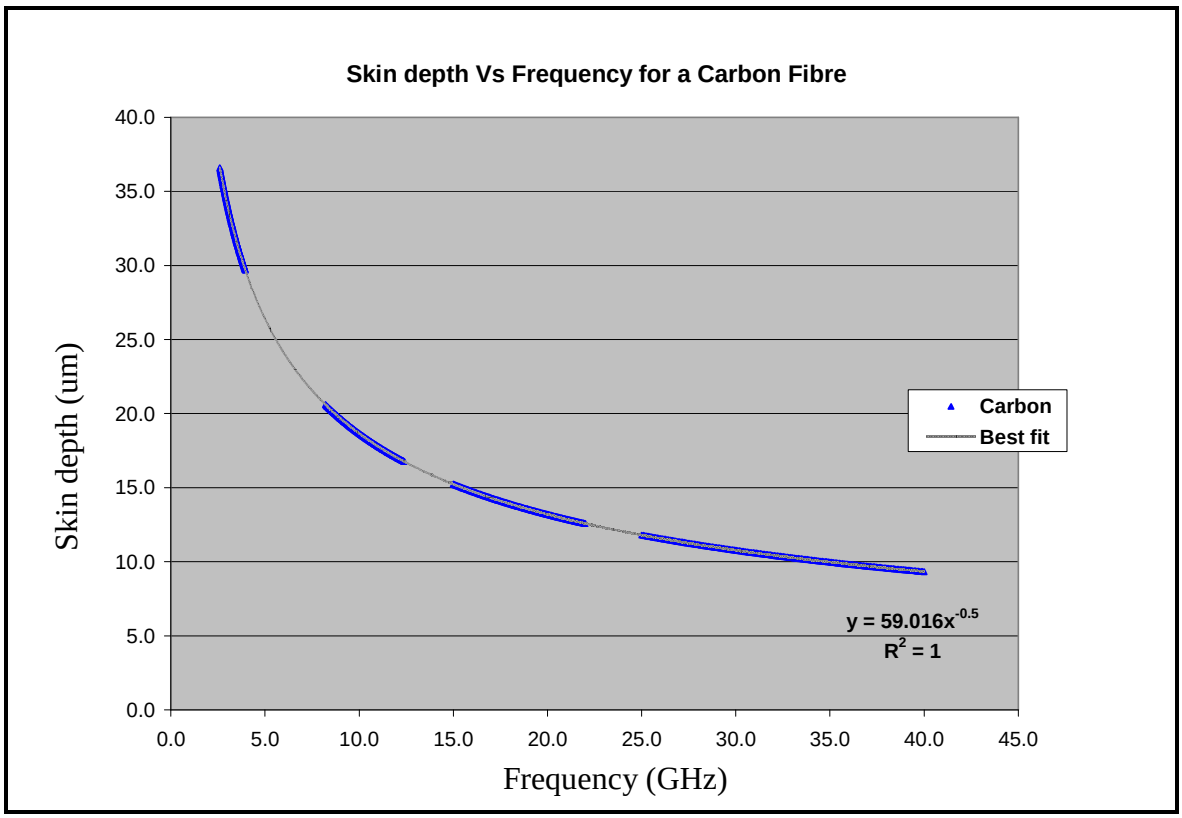

Figure 27: The dependence of Skin depth on frequency for carbon materials.

The graph shows that for frequencies 5 - 40 GHz the skin depth lies between 25 and 9µm. These distances are comparable to the veils thickness (particularly are lower basis weights) and so the skin effect is should be considered.

As the skin effect forces charge to the outer most surfaces, it then makes sense to make these surfaces as conductive as possible. By doing this, the amount of energy lost in the material is reduced, and the amount of shielding by reflection increases. This will be looked at in more detail in the next part of the report.

4.2 Effects of metal coating the carbon fibre

4.2.1 Introduction

This investigation will look at how the weight of nickel on the surface of the carbon fibre influences surface resistivity and SE of the nonwoven veil.

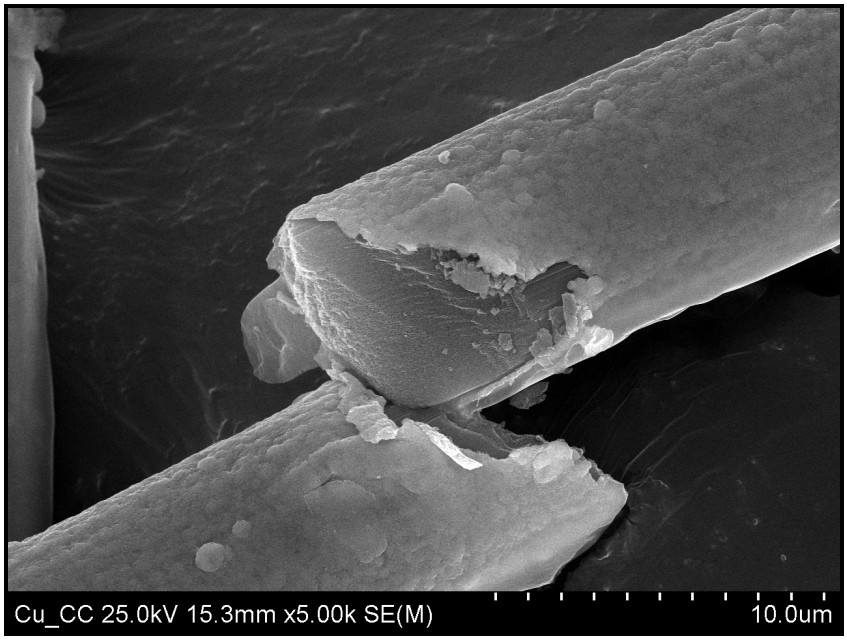

Figure 28: A fractured metal coated carbon fibre – the carbon fibre core and nickel coating can be clearly seen.

If we were considering exactly the same matrix with different weights of metal then we would expect to see that a greater coating of metal would result in higher levels of conductivity and therefore more shielding. However this experiment requires a careful approach. The matrix structure changes in a number of ways for each metal concentration considered.

For instance different weights of metal coating will result in a different number of fibres for a specific basis weight (see below). As we move from a heavily coated carbon fibre network to a lighter one, to obtain the same basis weight, a greater number of carbon fibres is needed (as the contribution of mass from the metal coating has decreased).

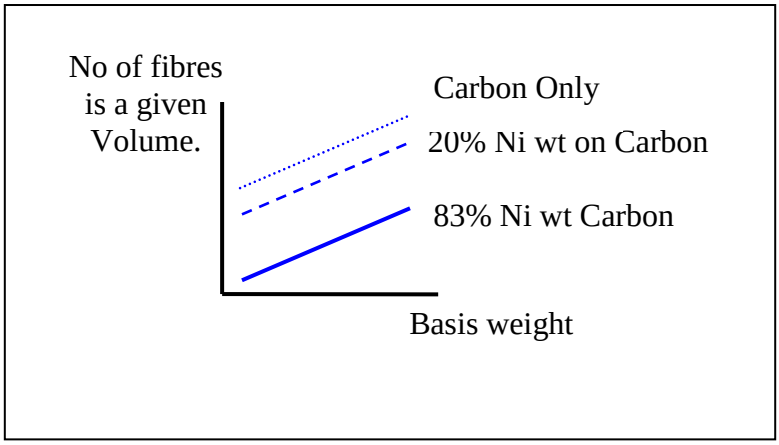

Figure 29: The effect of metal coating weights on the numbers of fibres, in a given Volume, for a range of basis weights.

This means that higher metal content veils will posses more porous structures, as seen in figure 30.

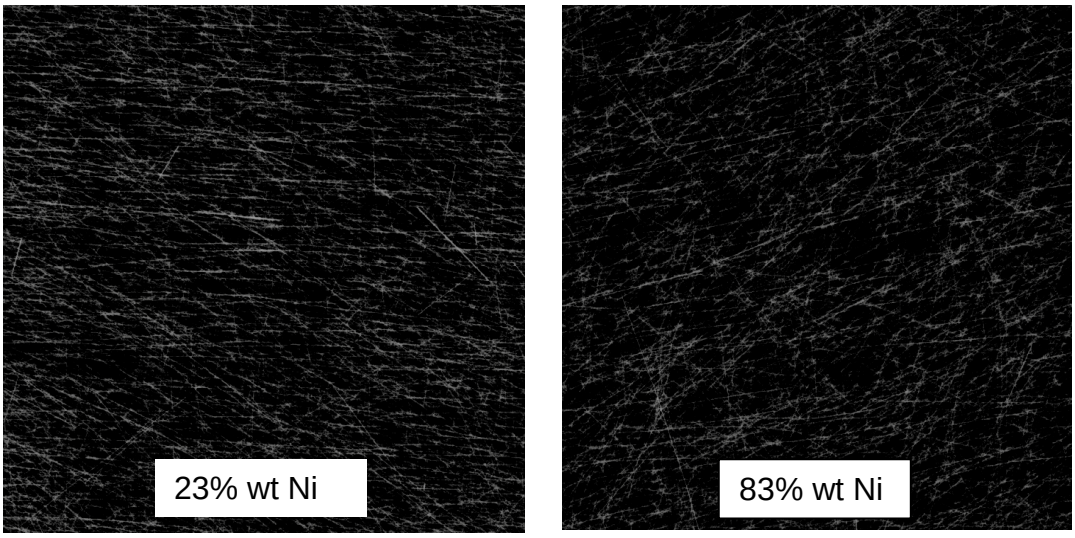

Figure 30: **Negative images of 23% and 83% nickel coated veil. Although not easy to perceive, the 83% nickel coated veil on the right is more porous.**

In this investigation a range of carbon coated veils was manufactured with different amounts of nickel coating by weight. The carbon fibres were coated using a metal coating facility (part of the TFP group) and then manufactured into veils on TFP's pilot line.

Nickel content	Basis weight tested	Fibre Length
23%	4, 10, 17, 34, 50, 75 and 100 g/m^2	12mm
40%	4, 10, 17, 34, 50, 75 and 100 g/m^2	12mm
60%	4, 10, 17, 34, 50, 75 and 100 g/m^2	12mm
83%	4, 10, 17, 34, 50, 75 and 100 g/m^2	12mm

Table 2: *The range of nickel coated concentrations and basis weights that have been tested.*

4.2.2 Results and Discussion

Firstly the materials were tested for formation quality to check if direct comparisons could be made (figure 30). Provided the formation quality was similar the materials were then analysed for Surface Resistance (figure 32) and SE (figures 33-34).

Formation Quality

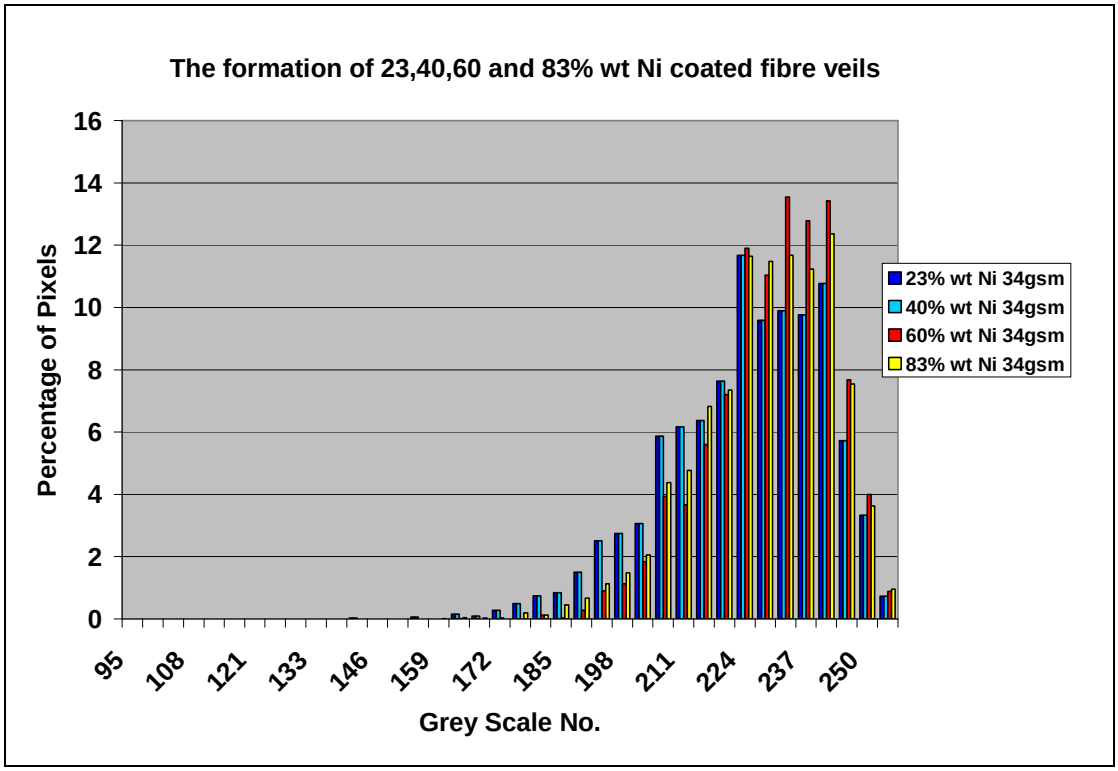

Figure 31: **The formation quality of 34gsm NiCC at various metal coating levels.**

The formation quality of each metal concentration for each basis weight was shown to be comparable – as *figure 28* demonstrates for the 34gsm materials *(graphs for other basis weights aren't shown for brevity)*. The profiles are similar, as was accommodated for by ensuring similar manufacturing conditions for each material.

The minor differences are that the heavier nickel coated fibres are shifted in the graph to the right (compared to the lighter ones) indicating a more porous structure as discussed earlier in section 3.7.

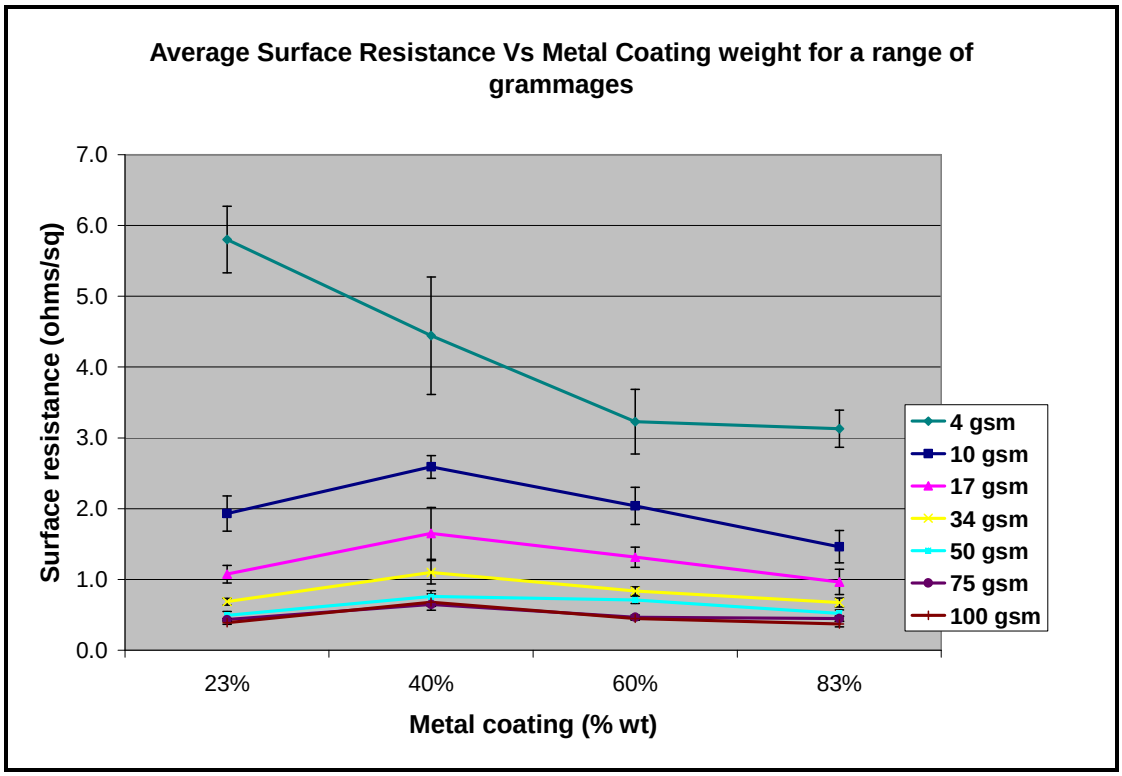

Figure 32: **The graph shows how the Surface Resistivity changes for different amounts of Nickel coating on the carbon fibre.**

A thicker metal coating on the surface of the fibre improves surface resistivity (for 40%, 60% and 80% samples). However the 23% nickel coated fibres display lower than expected Surface Resistivity values, upsetting this dominant trend. This is intriguing as one would expect the surface resistance of the 23% nickel coated carbon to be much worse than the 83% material, and this is not the case.

The metal level influences the Surface Resistivity of the lighter basis weights more significantly than that of the heavier ones. This is most easily demonstrated by comparing the extremes of the data set on the graph (i.e. 4 gsm versus 100 gsm) - 100 gsm trend line is relatively flat compared to the 4 gsm equivalent.

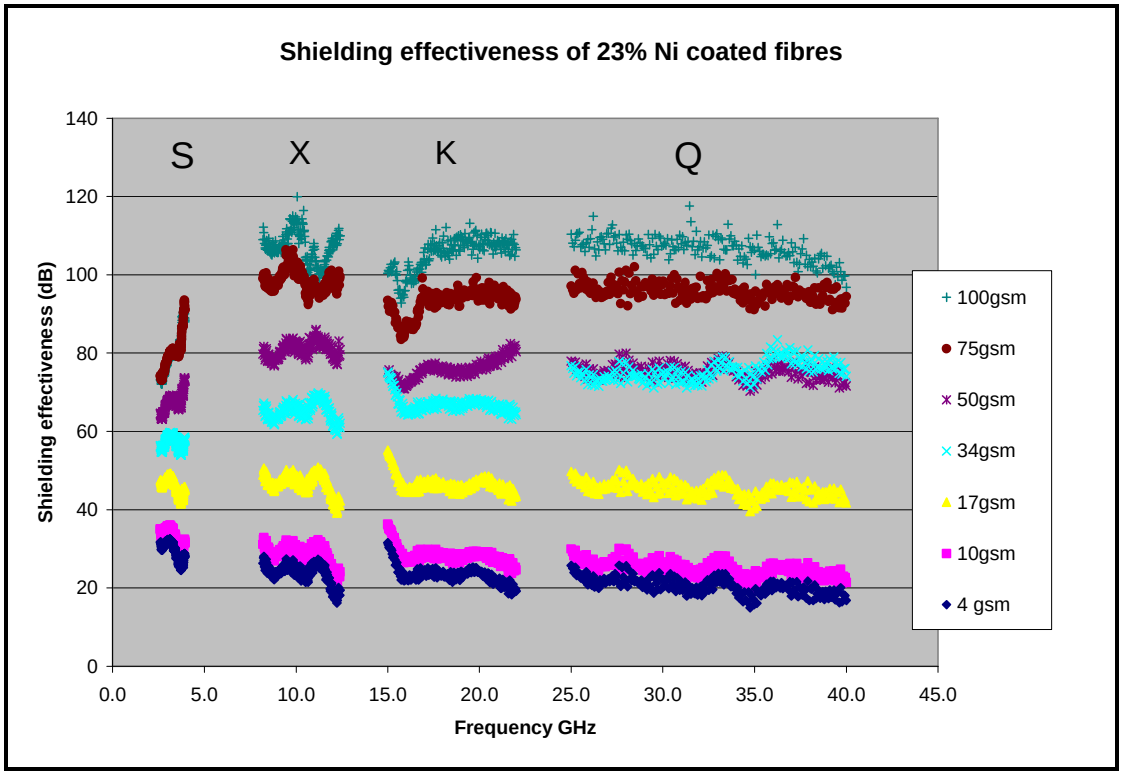

Figure 33: **The SE of 23% Nickel coated carbon fibres at a range of basis weights.**

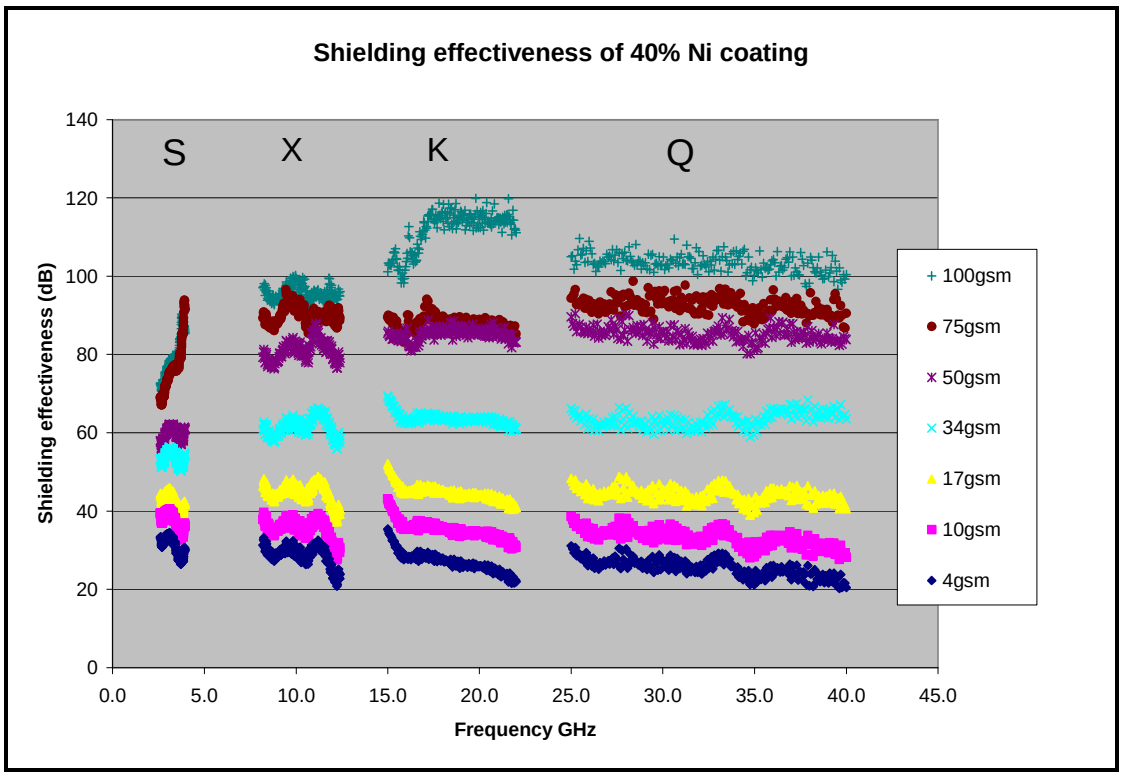

Figure 34: **The SE of 40% Nickel coated carbon fibres at a range of basis weights.**

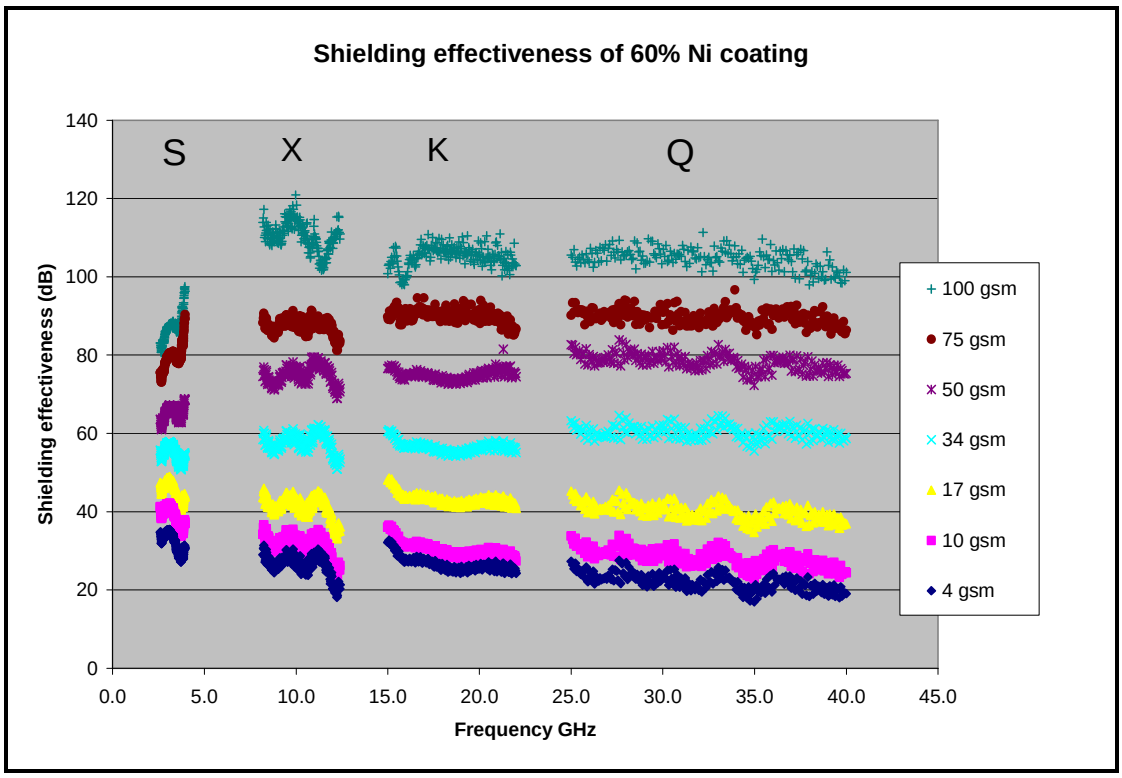

Figure 35: **The SE of 60% Nickel coated carbon fibres at a range of basis weights.**

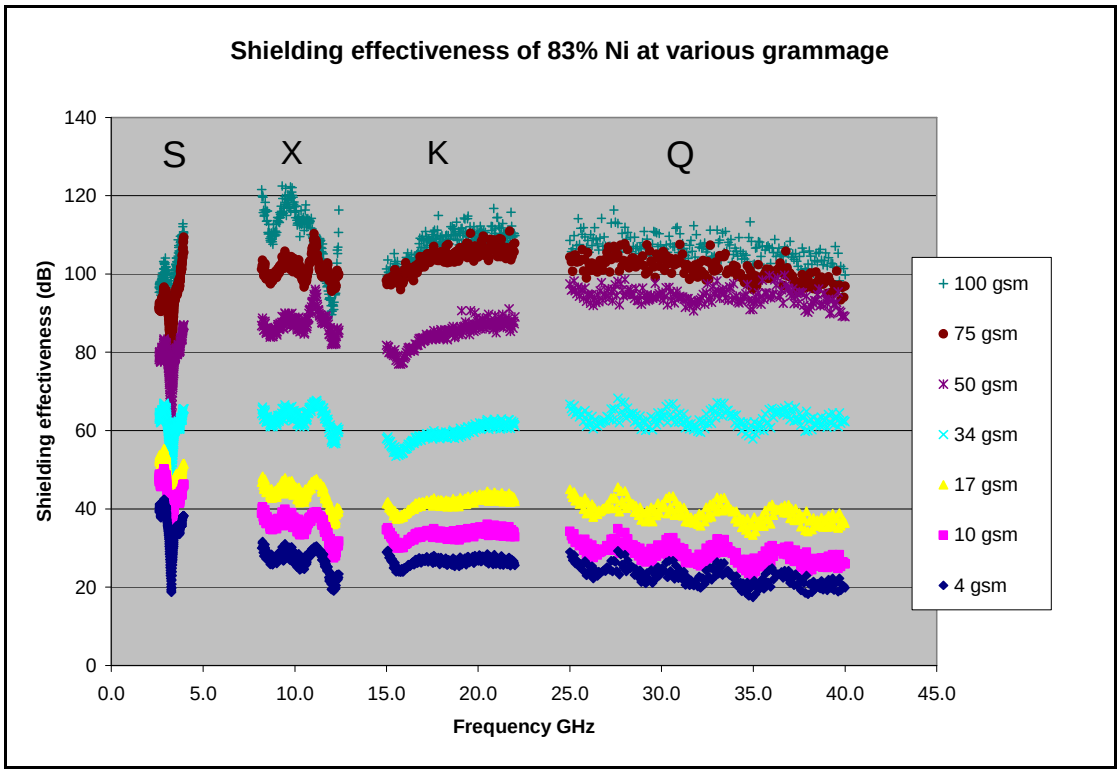

Figure 36: **The SE of 83% Nickel coated carbon fibres at a range of basis weights.**

The 23% wt nickel coated fibre veil shows consistent shielding across X, K and Q bands. S band shielding values are consistently lower (10±5dB) than the other bands for the heavier basis weights.

At 40% wt the SE of the lower basis weights (4, 10, 17gsm) remain constant (±5dB) as frequency increases. However their are some resonant effects to be found at the heavier basis weights (e.g. the 50 gsm X band and 100 gsm K band).

At 60% wt the lower basis weights (4, 10, 17gsm) show the SE falling (slight) as the frequency increases. This time we see a resonant effect in the 100 gsm X band.

The 83% wt S band regions show drastically improved shielding across all basis weights, thereby minimising the step usually observed between S and X bands.

Metal content can influence the SE, particularly at discrete frequencies (highlighted above). It can be concluded that for many of the lighter basis weights, changing the metal content does not appreciably affect the total SE.

As has already been demonstrated and discussed, increasing the metal content also has a major knock-on effect to the average pore size of the veil. The consideration that more metal = more conductivity = more shielding, does not hold true. This clearly demonstrates the importance of the other parameters that shielding is dependant on. To analyse this further, we must first consider the shielding mechanisms that dominate in a single veil.

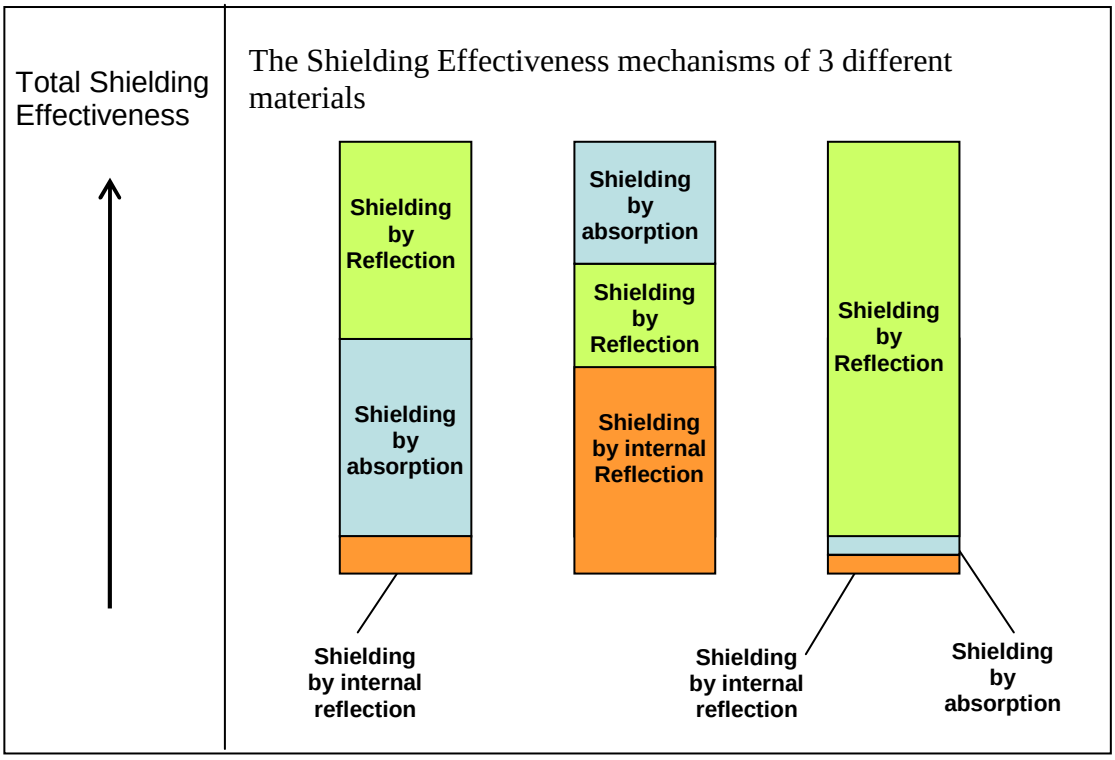

Figure 37: Potential SE mechanisms and their contribution to the total SE

Of the nickel coated carbon materials tested in this section, the most dominant mechanism of shielding is reflection, determined by measurement of the S-parameters S11 and S22. Additionally it can be shown that this result is expected theoretically. As the wave passes between two different media – that of air in the waveguide and that of the veil under test, the following description between the two media can be defined:

$$\Gamma = \frac{z_2 - z_1}{z_2 + z_1}$$

Where $\Gamma =$ Reflective coefficient

$z_1 =$ Intrinsic impedance of air $= \sqrt{\mu_{r1} / \varepsilon_{r1}}$

$z_2 =$ Intrinsic impedance of the veil $= \sqrt{\mu_{r2} / \varepsilon_{r2}}$

This shows that Γ is dependant on the ratios of μ_r and ε_r, and as the impedance of air is much higher than the impedance of the veil, high degrees of reflection are generated.
If the veil's intrinsic impedance were to be perfected matched to that of the propagation media (i.e $z_1 = z_2$) then the reflection $\Gamma \to 0$ and no reflection is generated.

4.3 Effects of changing Fibre length

4.3.1 Introduction

If a single carbon fibre that is 12mm long is compared to two 6mm fibres connected together using a typical (resistive) binder, the 12mm fibre proves to be electrically more conductive. It is evident that this is due to the fact that the binder acts as an insulating spacer between the two fibres.

Clearly identifying a 'conductive binder' would help solve this issue. Unfortunately identifying a water based binder that satisfies such conductive requirements is somewhat of a challenge. Various institutions are developing their own 'conductive binder' systems using nano-engineered polymers (e.g. using Carbon Nanotubes/Fibre [CNF/CNF]. *The use of such materials has also been studied parallel to this work*[16]

An alternative solution to this problem is to use longer fibres which reduce the numbers of insulative bridges required. Arguments along these lines assume that the conductive trends of a single fibre to fibre junction remain similar when integrated into one macroscopic object.

However the dispersion of longer fibres using TFP's current technology is challenging. Longer fibres tend to entangle causing clumps within the material, decreasing conductivity. Therefore an interesting constraint is set: the most conductive fibre network that can exist involves a balance between dispersion quality and the maximum fibre length. This limits fibre lengths to between 6 and 24 mm inclusive.

By optimising the veil for conductivity the SE should improve. This study will determine whether there is any noteable difference in the conductive and shielding properties of veils manufactured using different fibre lengths.

The experiment investigated four different fibre lengths over a full range of basis weights *(see below).* The nickel coated carbon fibres were manufactured into nonwoven materials using TFP's pilot line facility.

Fibre Length	Basis weight tested	Nickel content
6 mm	4, 10, 17, 34, 50, 75 and 100 g/m^2	44%
12 mm	4, 10, 17, 34, 50, 75 and 100 g/m^2	40%
15 mm	4, 10, 17, 34, 50, 75 and 100 g/m^2	42%
18 mm	4, 10, 17, 34, 50, 75 and 100 g/m^2	43%

Table 3: *The range of fibre lengths and basis weights that have been tested. As there was a requirement to use out of Specification fibres, a slight Nickel content variation was unavoidable.*

4.3.2 Results and discussion

The results obtained by measuring the formation quality, Surface Resistivity and SE are discussed below.

Formation quality

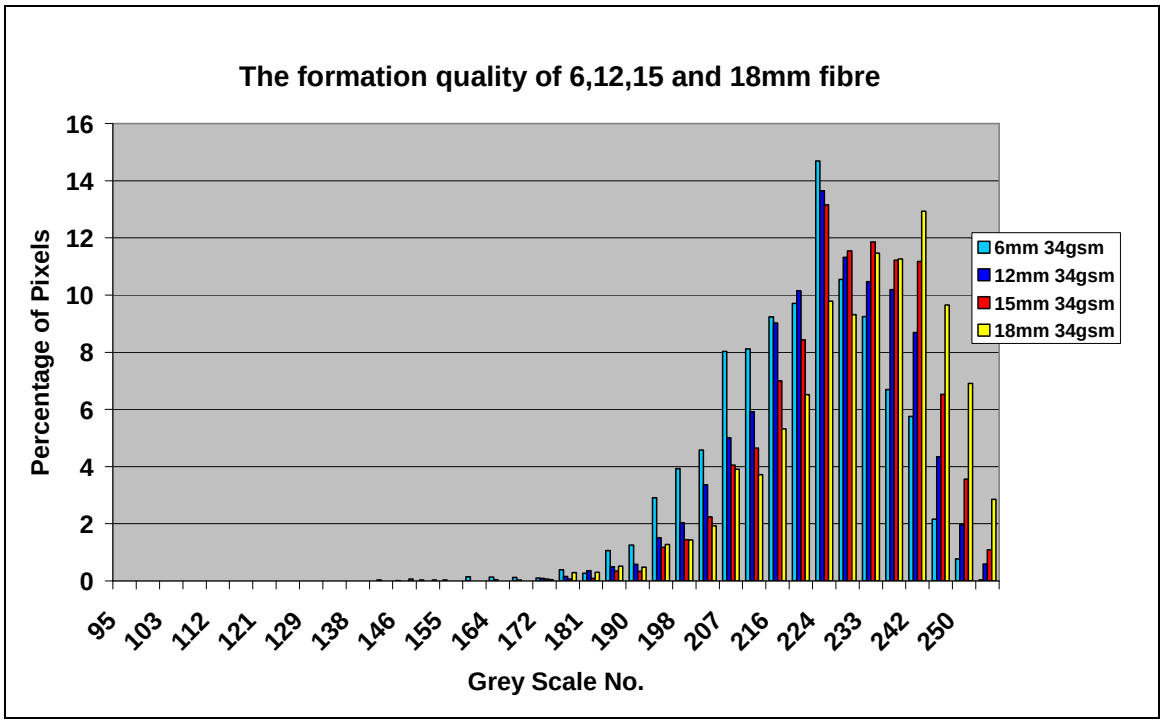

Figure 38: **The formation quality of the 34gsm NiCC at a range of fibre lengths.**

The graph shows that the formation quality of the samples was similar. However the sharper peaks of 6mm/12 mm compared to 15mm/18mm show better dispersion characteristics at lower fibre lengths. The 18mm's profile is widest, resembling the poorest formation fibre length as expected.

Surface Resistivity

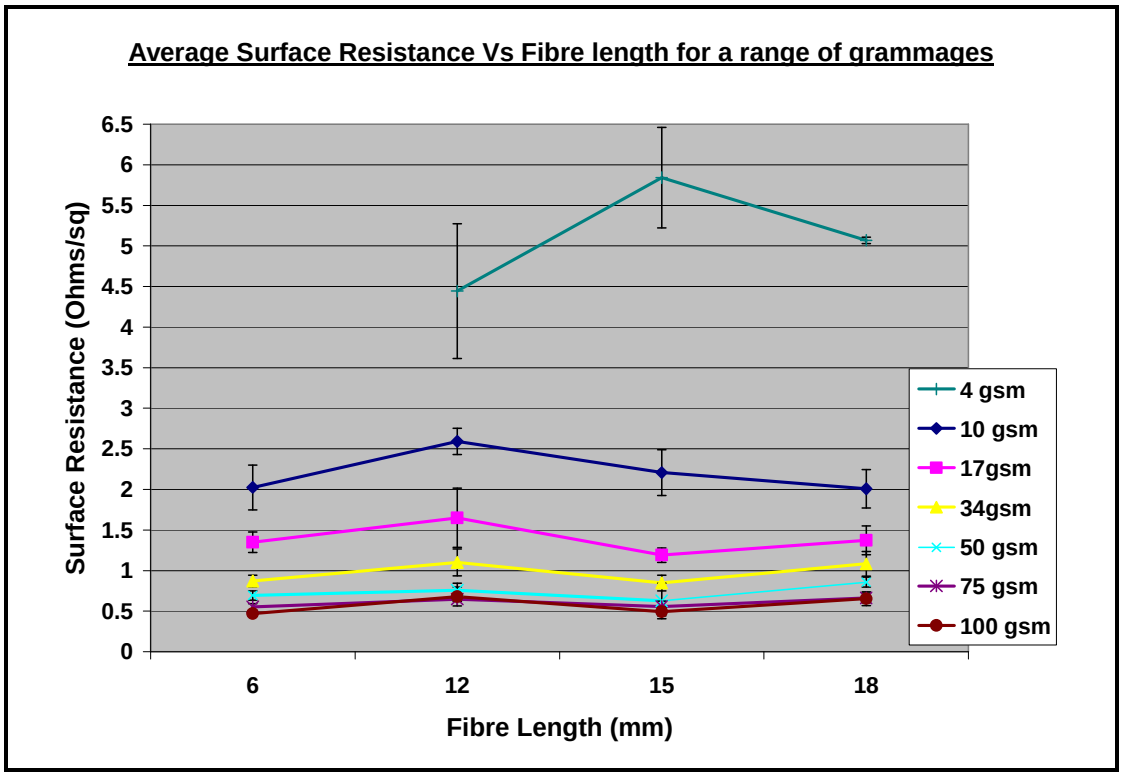

Figure 39: **The Surface Resistivity of 6, 12, 15 and 18mm fibres at a range of basis weights. The 4gsm 6mm material could not be manufactured due a lack of tensile.**

The graph shows the familiar trend - higher basis weights display lower surface resistivity. This again can be attributed to the increased numbers of fibres embedded within the matrix, allowing electrical charge to be conducted more efficiently.

The effects of fibre length on Surface Resistivity are more difficult to visualise. This is partially due to the dispersion differences between the fibre lengths.
Fibre length does not significantly influence Surface Resistivity at heavier basis weights, although its effects are more noticeable at 4 and 10 gsm materials.

If the 4gsm material is ignored, we can see that 12mm fibres display the highest values of Surface Resistivity within all basis weights. Conversely 6 and 15 mm fibre lengths consistently show higher levels of conductivity, and therefore they should be selected when the highest levels of conductivity are required. From earlier predictions this result was not expected.

SE

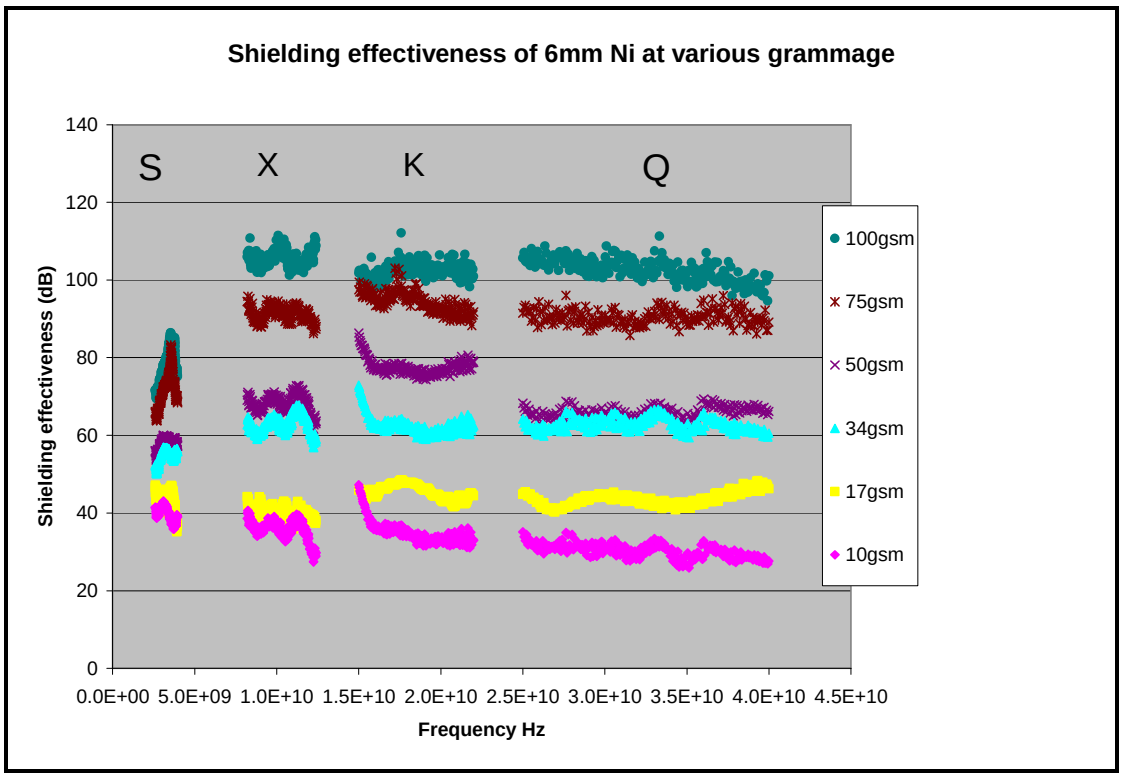

Figure 40: **The SE of 6mm, 10 – 100 gsm NiCC**

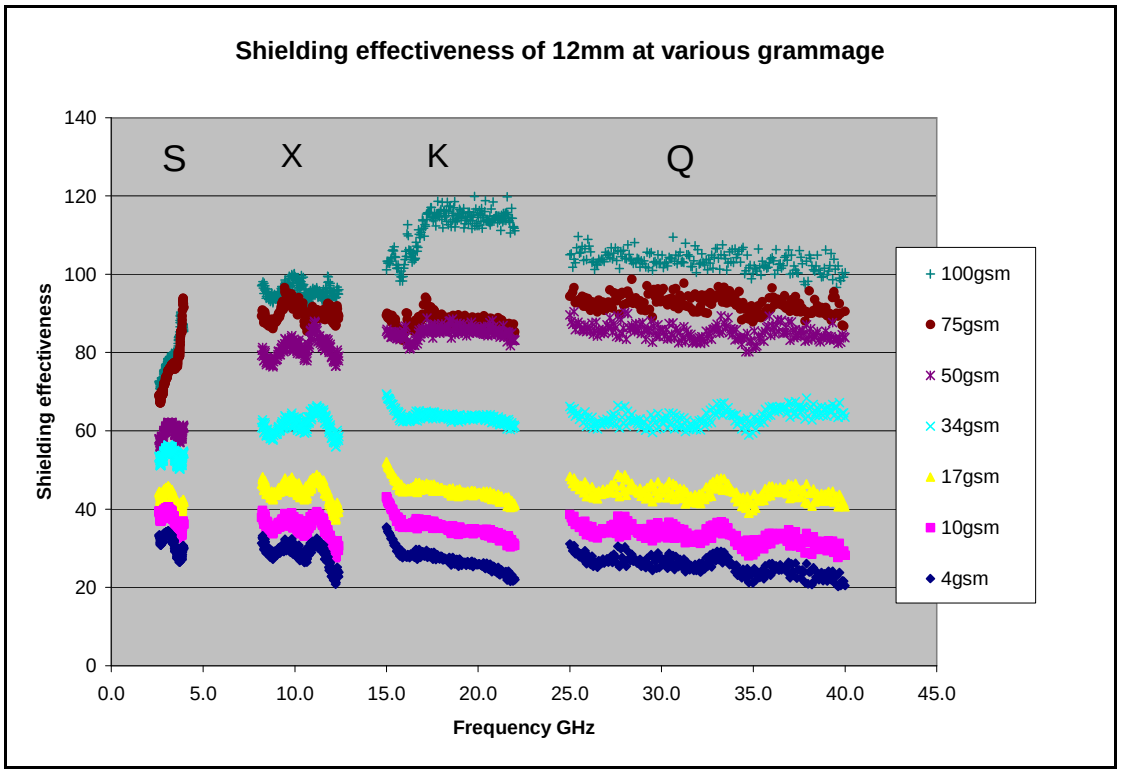

Figure 41: **The SE of 12mm, 4 – 100 gsm NiCC.**

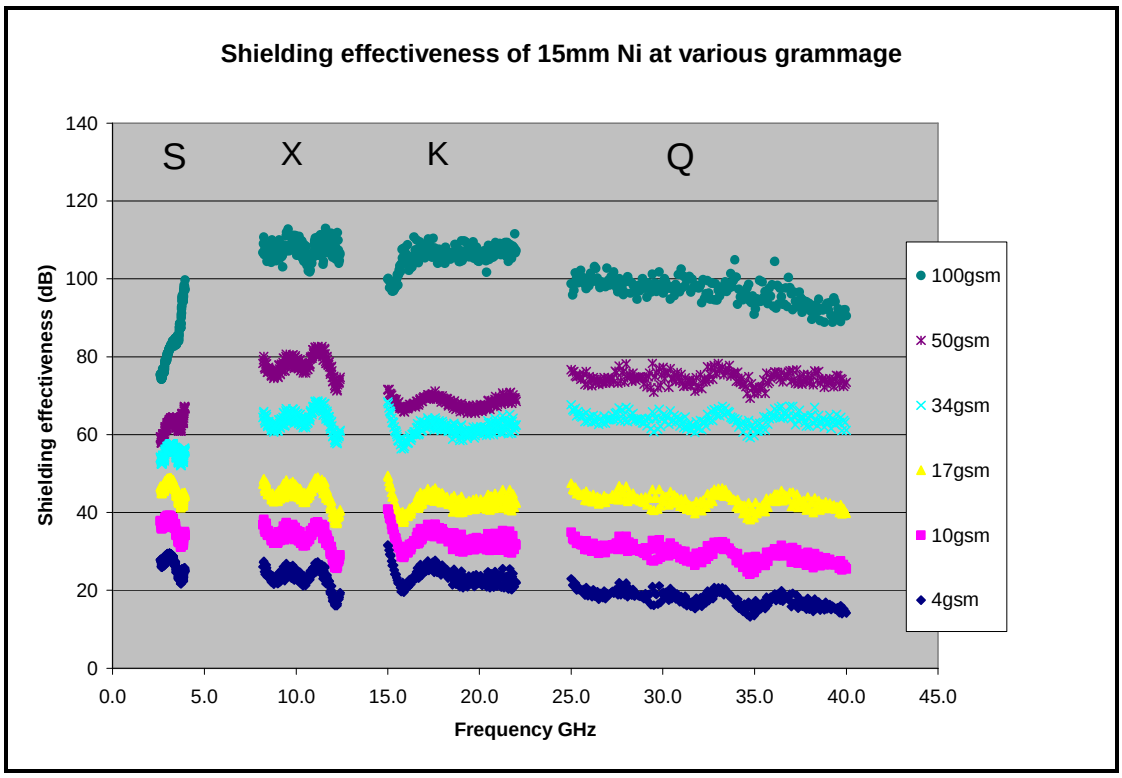

Figure 42: **The SE of 15mm, 4 – 100 gsm NiCC.**

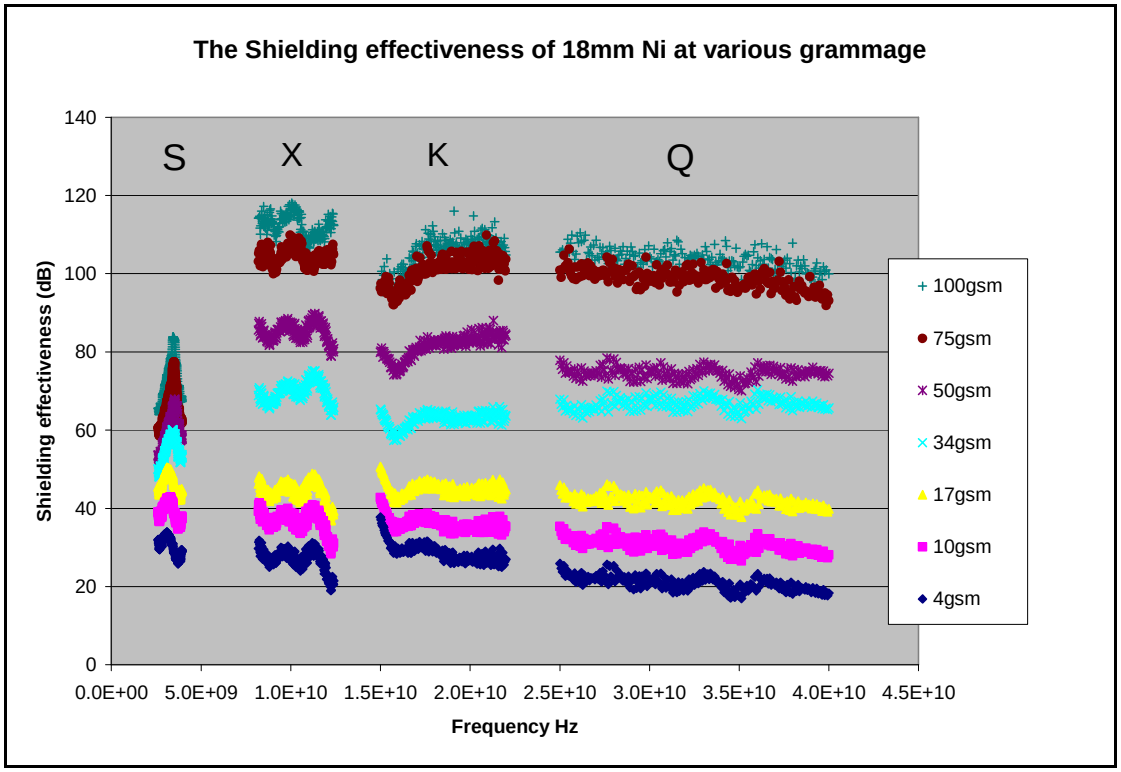

Figure 43: **The SE of 18mm, 4 – 100 gsm NiCC**

.

From the graphs above, it is difficult to perceive any significant differences in the SE for 6, 12, 15 and 18mm fibres. For instance, the maximum observed change in SE for different fibre lengths was 10±5dB, whereas differences in basis weight can influence the SE by as much as 100±5dB. Having said this, certain resonances do exist (eg the 12mm, 100gsm K-band values) which could serve as performance 'boosts'.

If sample variability and mismatch ripples[E] (seen running throughout the data sets) are also taken into account, this study shows that for most frequencies and basis weights, the fibre length has a trivial effect on the total shielding performance of the veil. It is believed that poorer formation quality of the longer fibre veils is offsetting the inherent electrical advantage (discussed in the introduction of this study).

[E] The 'mismatch' ripple will be discussed further in section 7.1.

4.4 Effects of multiple metal coatings on carbon fibre

4.4.1 Introduction

Copper/nickel (CuNi) coated carbon fibre veils currently represent TFP's premium product for conductive applications such as EM shielding.

This investigation considers CuNi coated fibres (60% by weight) that were manufactured into nonwoven veils, on the pilot line. A range of basis weights were produced from 4 – 100 grams per square meter (gsm). These materials were subsequently tested for Surface Resistivity and SE.

4.4.2 Results and Discussion

The results obtained by measuring the Surface Resistivity and SE of the CuNi veils are shown below in figure 44 and 45 respectively.

Surface resistivity

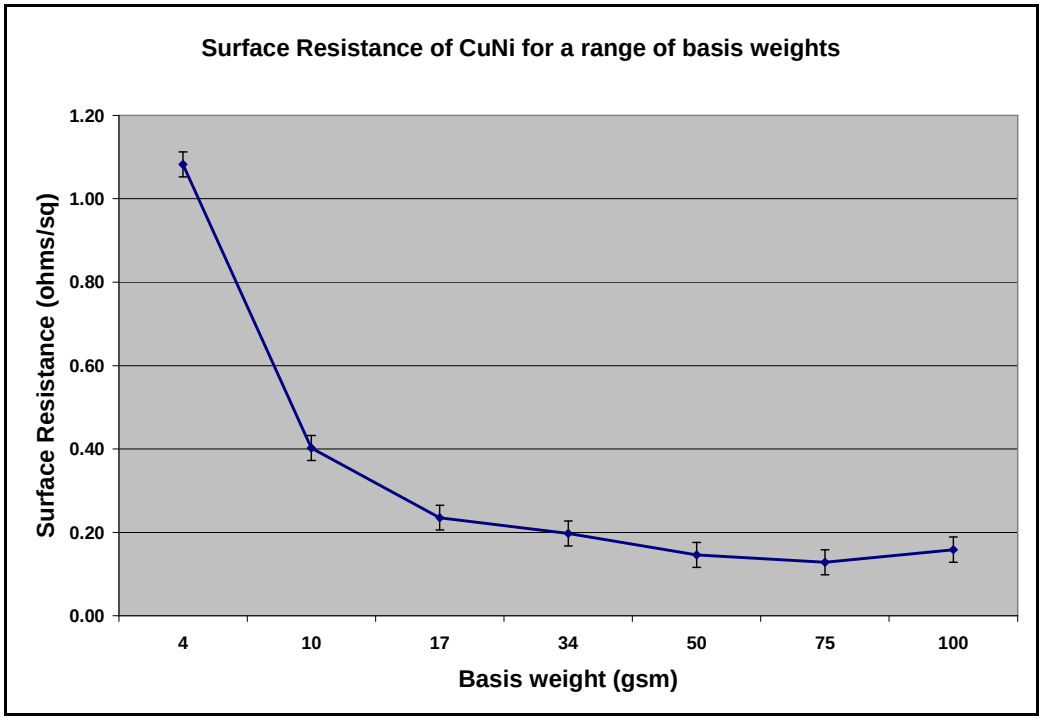

Figure 44: The decrease in Surface Resistivity with increasing basis weight.

The graph shows the decrease in surface resistivity as the basis weight increases. This effect is attributed to the increased numbers of fibres embedded within the matrix, allowing electrical charge to be conducted more efficiently (and therefore at lower

resistance. The 100gsm material displays slightly higher levels of resistance than would be expected.

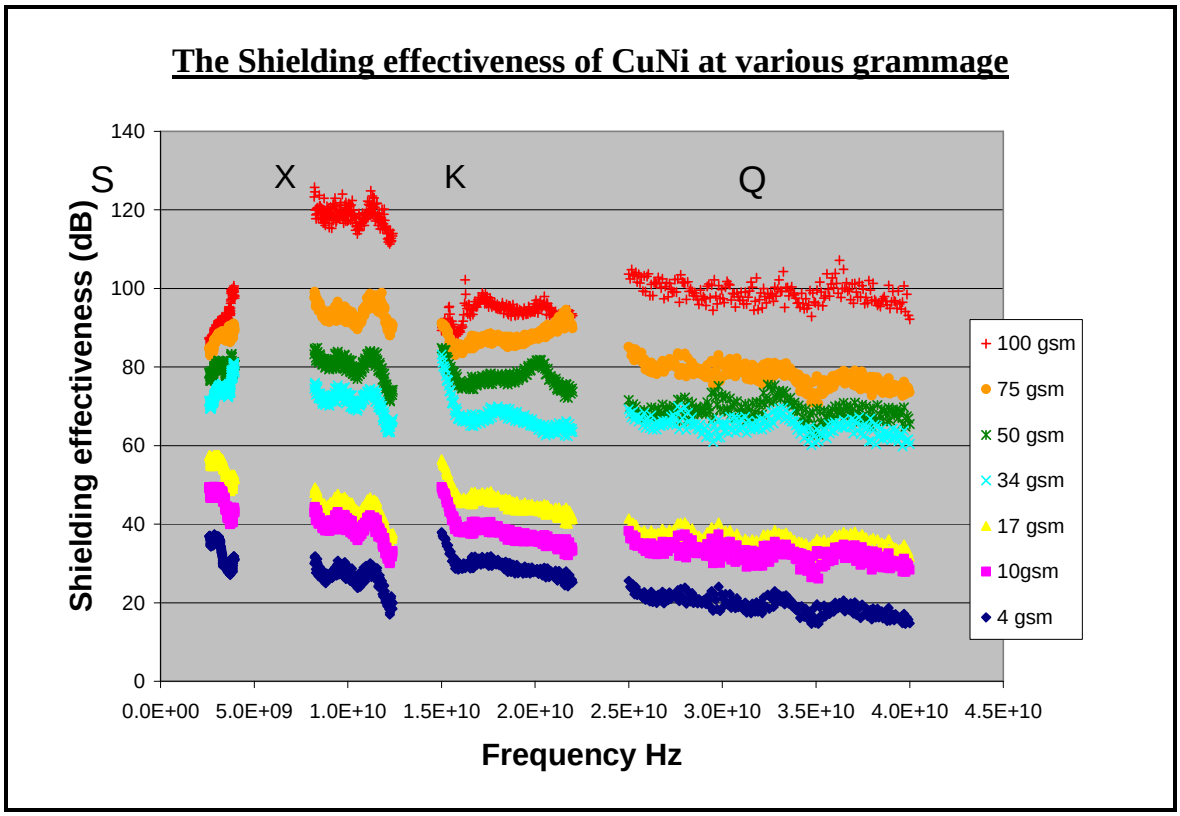

Figure 45: **The SE of CuNi coated carbon fibre at various basis weight.**

The CuNi coated carbon veils show frequency specific shielding performance, with the higher basis weight veils shielding most effectively. The graph contains a 'valley' which separates the veils into 2 main groups – 4, 10, 17gsm and 34, 50, 75, 100gsm.
At heavier basis weights (particularly 100 gsm) optimum shielding is obtained at X band frequencies (8.2 – 12.4 GHz). However lower basis weights peak shielding performance occurs at S band frequencies (2.6 - 3.95 GHz).The lower basis weight materials resemble that of traditional metal films, with shielding performance decreasing as frequency increases. It is believed that this effect is partly caused by the skin effect.

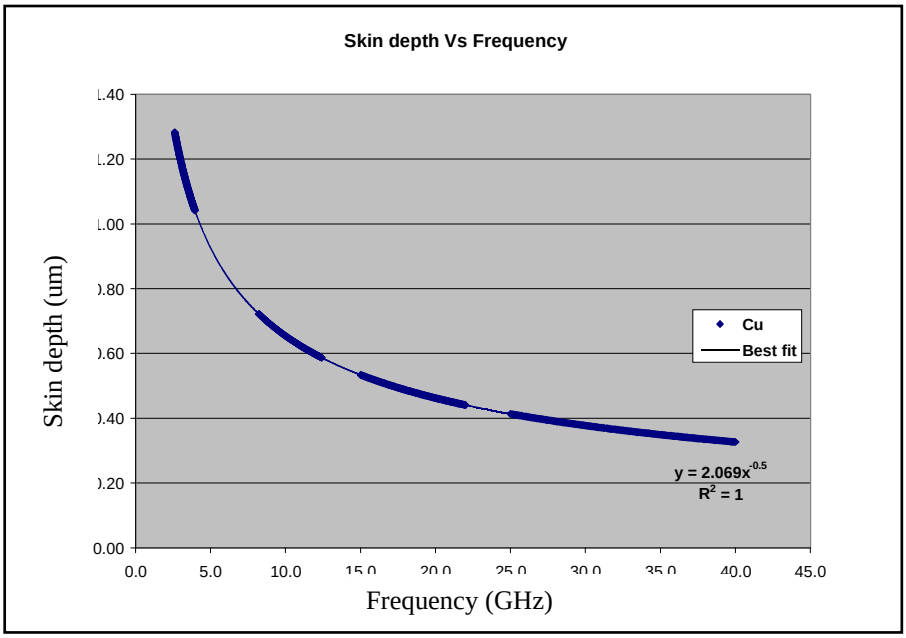

Figure 46: The dependence of Skin depth on frequency for copper coated materials.

4.5 Effects of particulate addition to the veil matrix

4.5.1 Introduction

It was postulated that the addition of micron sized metal particulates into the surface of the veil may increase conductivity and yield EM shielding benefits. Preliminary studies have validated this and it was shown that the degree of conductivity and shielding increase was dependant on 4 main factors:

- The type of particulate
- The amounts of particulate
- The particulate orientation particularly in the case of thin or flake like material
- The method in which the particulate is incorporated into the veil

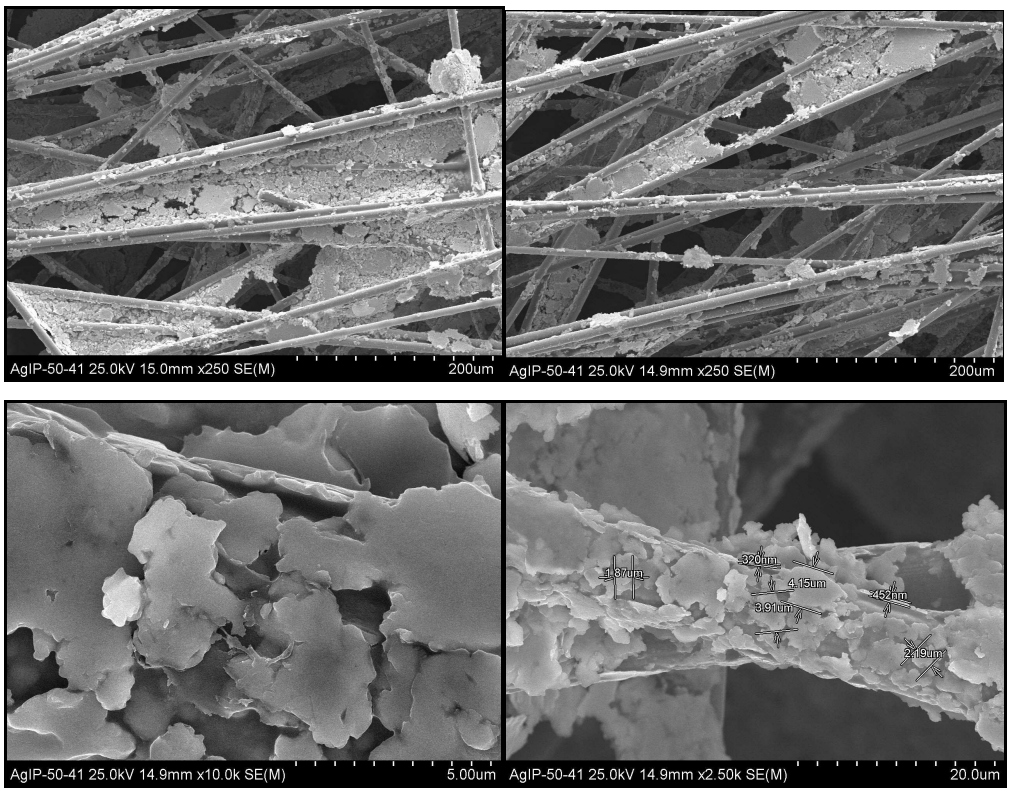

Figure 47: Silver particles encapsulated by the nonwoven structure (magnification X250)

In this study five different types of particles were studied (table 4). The particles were used in their 'as supplied' form, which means that when considering the results one should keep in mind the original metal contents defined below.

Metal Particle loadings	**As supplied Metal content *(% by weight)***	**Additional information**
Copper Zinc alloy *(GoldBronze 3001)*	100%	Copper/Zinc Alloy Flakes d50 = 20 μ m
Aluminium *(StarBrite 5102)*	10%	Aluminium Flakes d50 = 12 μ m
Iron *(L-11859)*	90%	Iron Flakes d50 = 13 μ m
Silver *(Tl-412A)*	44%	Silver particles d50 = 9 μ m
Stainless Steel *(RMT 442)*	70%	Steel particles d50 = 31 μ m

Table 4: A listing of the particle type/*trade name*, the 'as supplied' dispersion concentration and any additional information such as the average particle size (d50).

These materials were prepared and applied to the nonwoven veil in the laboratory[F], and then analysed for their SE. Finally the amount of particle addition was optimised using a statistical package called 'Statgraphics'.

[F] Further details of particle addition and the making of the basesheet can be found in appendix 8.4

4.5.2 Results preamble

Statgraphics, Design of Experiment and Response Surfaces

Statgraphics is a modelling tool that enables the use of 'designed experiments'.
A designed experiment (such as a 'Box-Behnken') enables us to vary 3 parameters simultaneously and interpret the results on a single response variable (such as SE). The advantage of using such a design means that far fewer samples have to be manufactured, and response plots can be created. The 3 parameters chosen to be analysed were:

1. Metal particle loading weight (as supplied from the manufacture).
2. Veil basis weight.
3. Binder concentration.

The effects of each of these parameters on the SE (the response variable) can then be plotted as a response surface (figure 49). An example can be seen below:

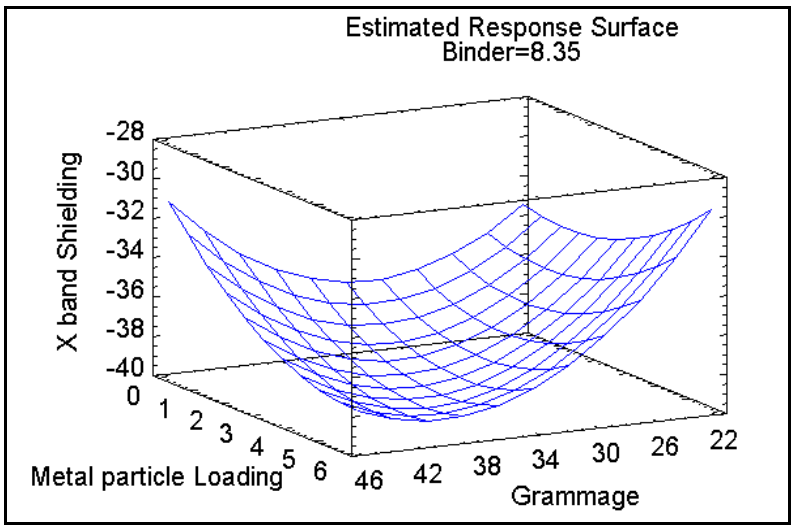

Figure 48: An example of a SE response plot based on the variables grammage, metal particle loading and binder.

The scales for the axis of this graph (and the ones that follow) are:

Metal particles are measured in grams,(g)
Grammage measured in grams per square meter (gsm)
Shielding in decibels (dB).

4.5.3 Particulate addition: Results

In this study Shielding Effectiveness has been defined as a negative quantity. Therefore a more negative value infers a greater amount of shielding (converse to the graphs earlier in this report). This was unavoidable due to predefined definitions within Statgraphics.

Copper Zinc alloy (GoldBronze)

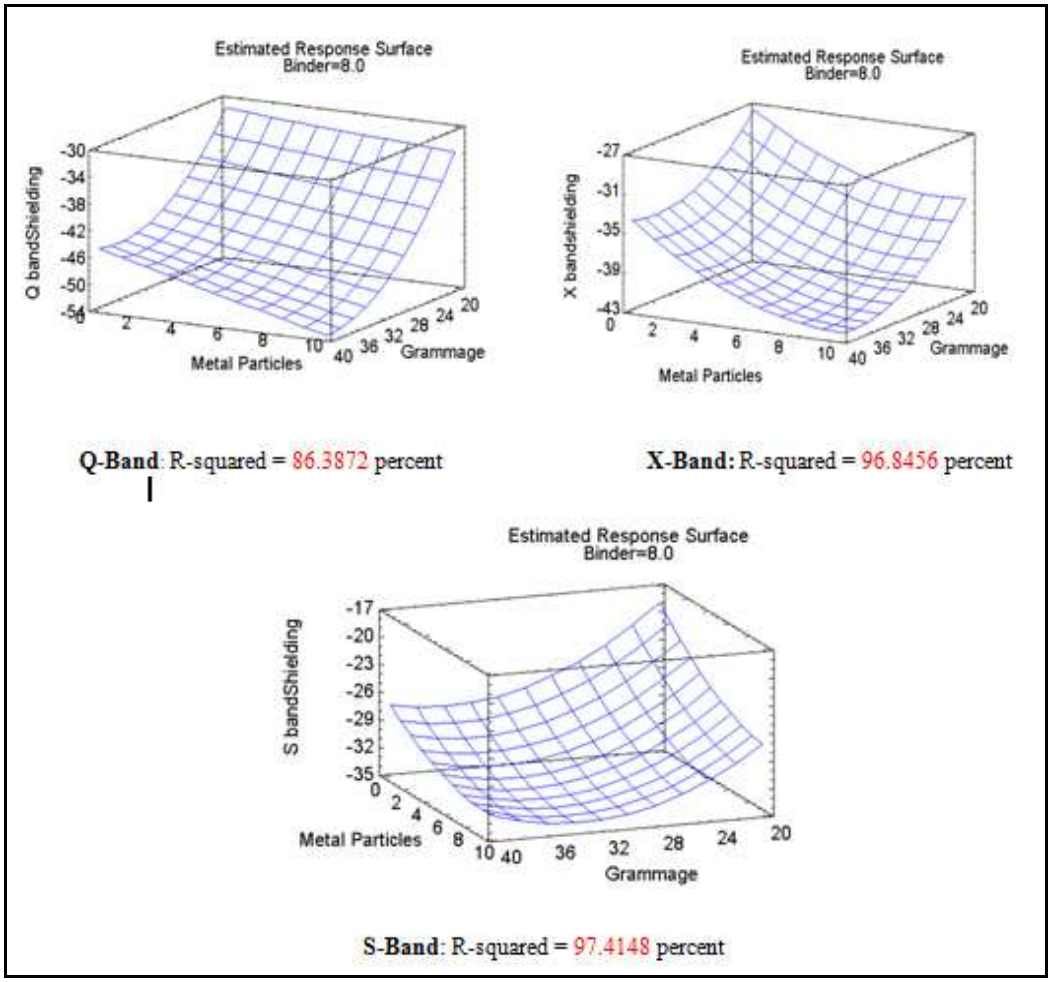

Figure 49: The response surface plots the Copper Zinc alloy particulates. The graphs were produced using Statgraphics and 'design of experiment' methodology.

All three response surfaces show optimised results at heavy veil grammage and metal loading. The R-squared values show how accurately these models represent the data. Shielding is highest in the Q-Band, moderate at X-Band, and poorest at S-Band.

The binder is the least significant variable and therefore it has been chosen to be fixed constant whilst the other 3 parameters (Shielding, Metal particle addition and Grammage) are all varied.

Aluminium (StarBrite)

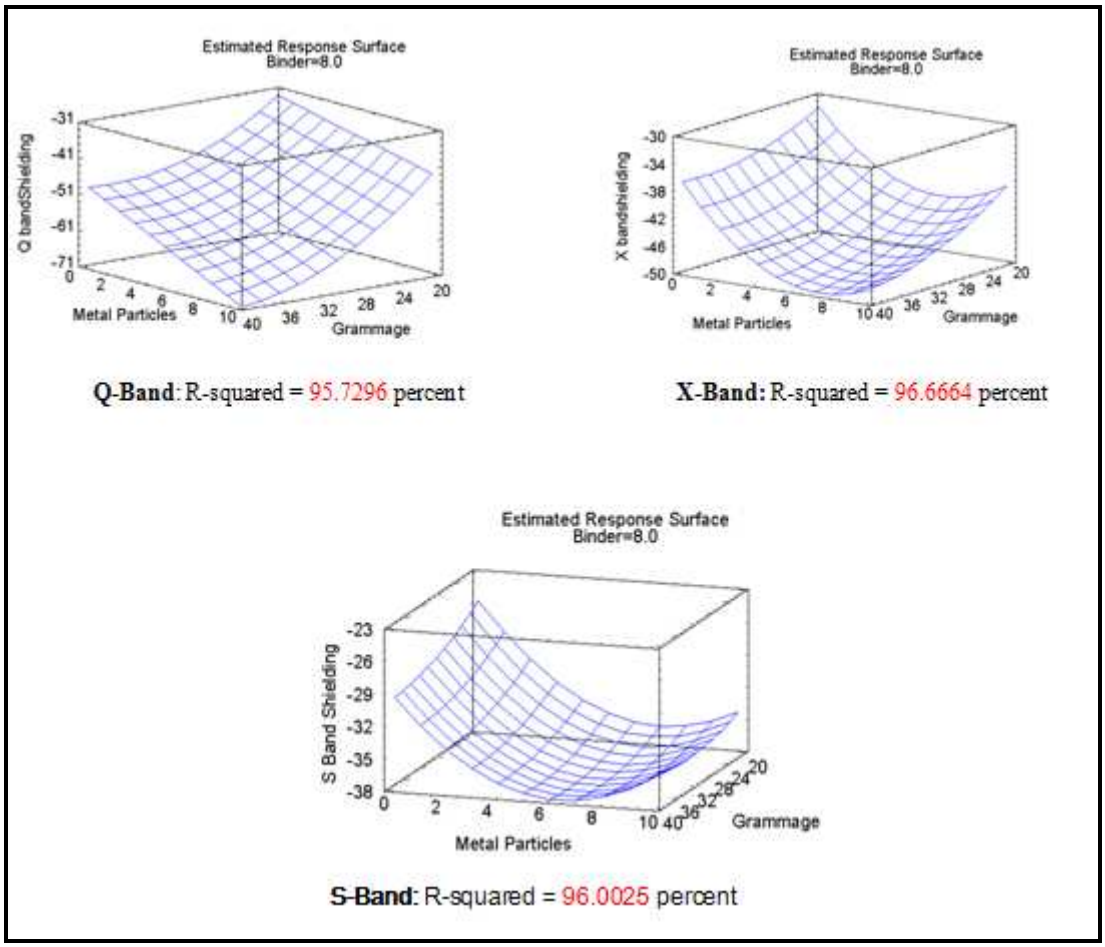

Figure 50: The SE response surfaces for Aluminium loaded veils.

StarBrite shows a similar distribution with regards to veil grammage, with increases in shielding found at higher grammage. However the particle loading influences X and S-band shielding the most when around 7grams (0.7grams of Al) of Starbrite is applied. This could due to optimum dispersion conditions at this particular loading. The high R-squared values for all 3 frequencies show strong trend correlation.

Iron (L-11859)

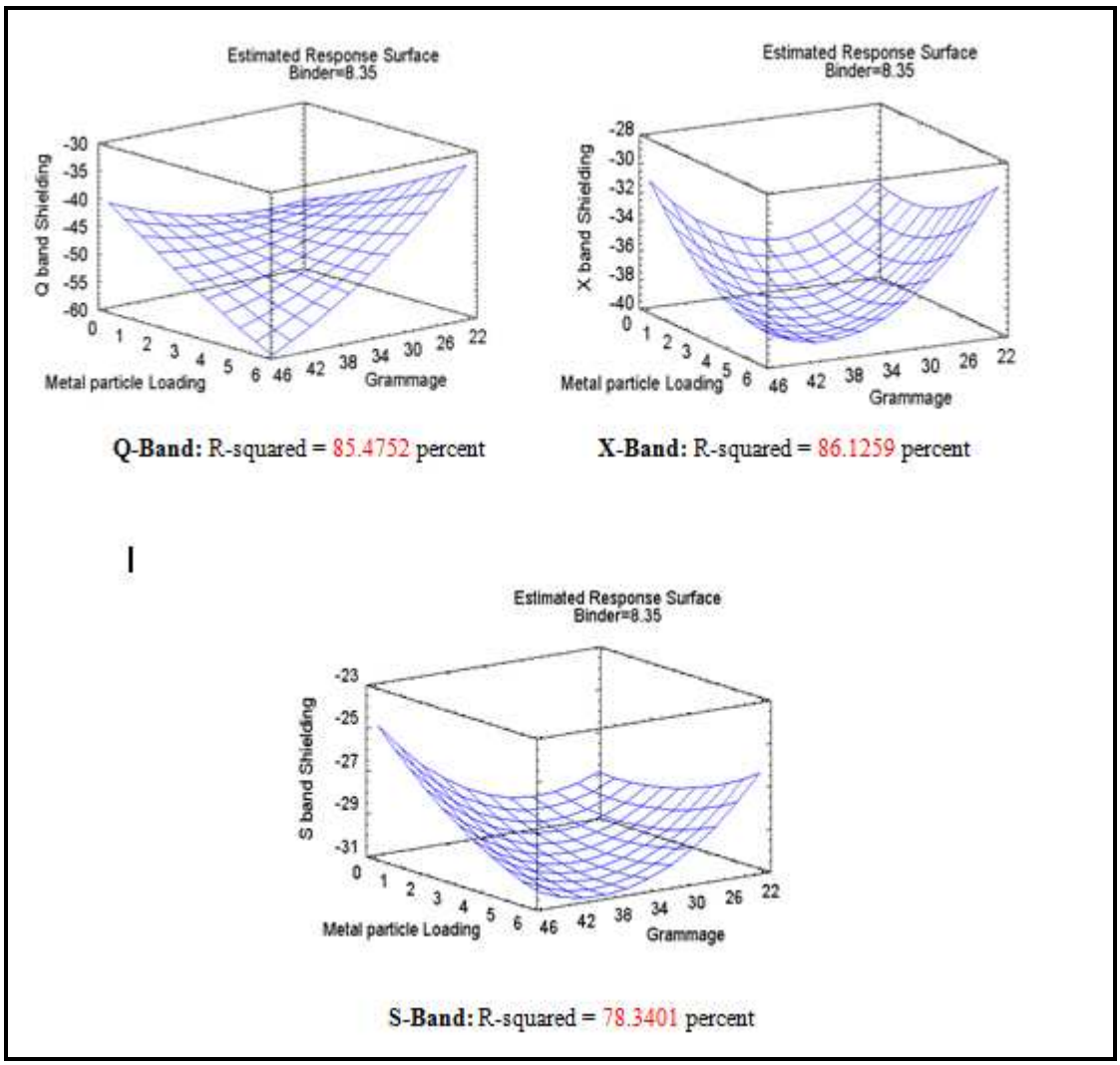

Figure 51: The SE response for Iron loaded veils.

Iron SE performance shows a strong dependency on the specific frequency band it is analysed over. Q-band shielding performance is significantly stronger than X and S-bands, contrasting the Goldbronze samples. Heavier Iron loadings produce higher shielding values at all frequencies, as expected. R-squared values for these mappings are lower compared to the other samples, resulting in the response surface fits being less accurate.

Silver (Tl-412A)

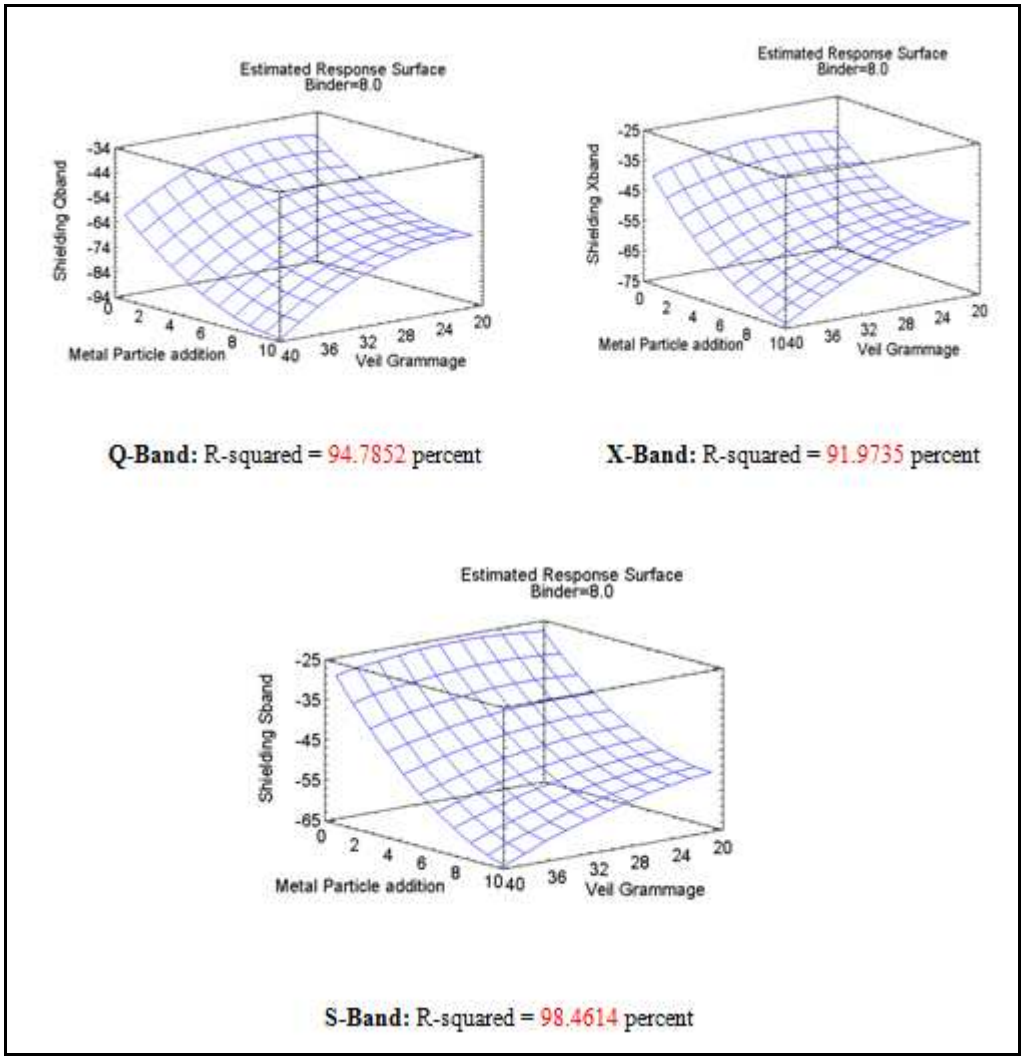

Figure 52: Optimised SE response for Silver loaded veils.

Silver exhibits the highest shielding performance within these groups at all frequencies. Up to 95 dB can be see in the Q-band range. R-squared values are also very high indicating a strong response surface fit.

Stainless Steel (RMT 442)

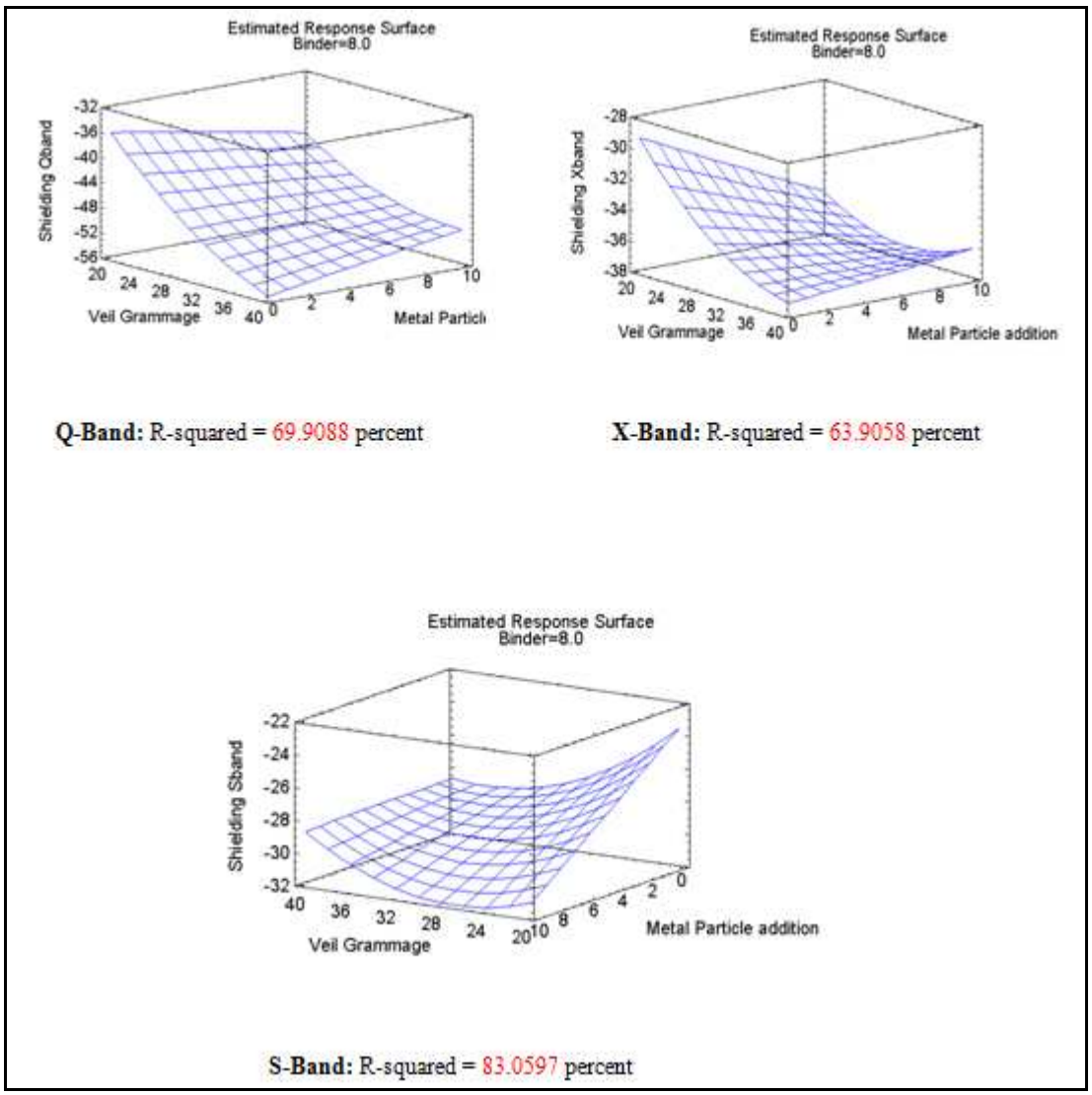

Figure 53: Optimised SE response for Stainless steel loaded veils.

Stainless Steel shows lower levels of performance shielding, which are similar to those of Iron. R-squared values are lower than 90% indicating poorer response surface fits.

Group Comparison

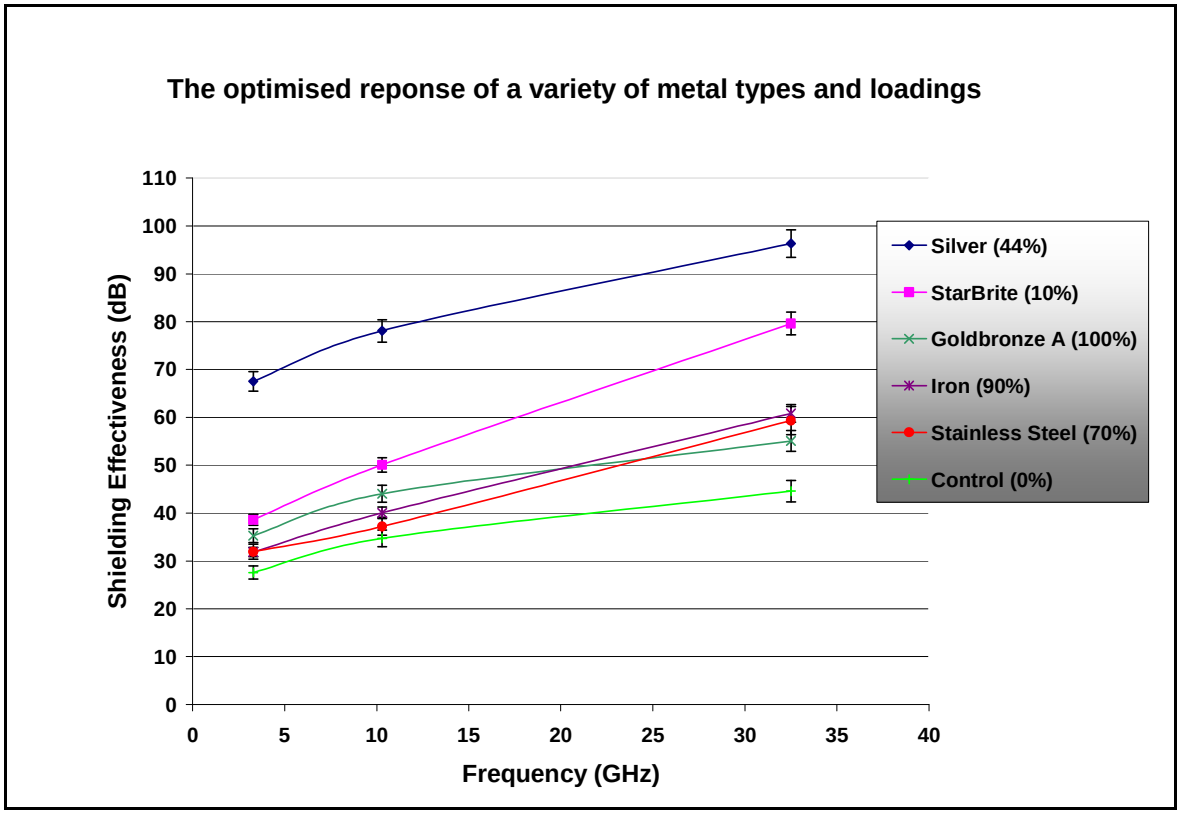

Figure 54: The optimised SE values that each metal addition (once optimised) brings.

4.5.4 Discussion

Figure 54 highlights the performance increase that is possible by adding silver particles. Aluminium (StarBrite) shows the second highest shielding value in the Q and S-bands. This is an impressive result as the aluminium samples only contain 10% metal particulates.

Veil grammage and metal loading are the key influences on the SE. Both higher grammage base veils and higher metal loadings show increased levels of shielding. Although binder content wasn't as a significant parameter, it still had an influence. Particularly when applied at such a sufficiently high or low quantity that more extreme effects were observed. These extreme effects range from SE deterioration to complete sample failure.

In the future it would be desirable to repeat this experiment with particle dispersions that were similar in nature, i.e. similar particle size, carrier system and metal content amounts. It is true that metal contents could have been scaled to ensure equal loadings, however aluminium quantities made that option not possible. Additional improvements to this

experiment would involve the testing of more conductive binder systems, as it is believed this would have a positive impact on the conductivity.

4.6 Error analysis

Common to all the shielding data in this study, there is a mismatch ripple that produces variations in the absolute SE value at any one frequency. It has been shown that this variation is repeatable and for each sample is purely a function of the experimental setup and not that of the material under test.

In this study a simple 'through port' calibration technique was used, which doesn't correct for simple phase changes caused by the addition of the material under test, or the slight movement of a wire. Additionally, reflections from the waveguide walls, sample resonances and transmission loading all contribute to the error associated with the SE values. More advanced calibration techniques have been identified (TRL[G]) and they will be discussed in the future work of this report, section 7.

[G] TRL (Through, Reflect and Line) refer to a more advanced calibration method which accounts for phase errors, producing results with less variance. See section 7.1.

5 Summary and Conclusions

This study has reviewed the current understanding, theory and practises that exist in the domain of electromagnetics, electromagnetic shielding and shielding test methods.

Although a sound theoretical understanding of electromagnetics, and to a lesser extent EMI, has existed for some time, there is much less information available in relation to the shielding test methods. To research this effectively, site visits and meetings were required, often with Defence organisations such as Selex Gallileo and BAE Systems.

The study then presented a collection of experiments and results, relating to modified nonwoven materials, including quantifying the effects of: Basis weight, Fibre length, Metal coatings and particulate addition, on electrical conductivity and Shielding Effectiveness. Although certain parameters (such as fibre length) were shown not to give a performance benefit, other variants displayed increased electrical conductivity and Shielding Effectiveness (such as the particulate modified veils).

Optical scanning analysis, scanning electron microscopy and energy-dispersive X-ray spectroscopy provided a strong qualitative analysis which was particularly valuable in gaining an insight into particle condition and distribution within the nonwoven structure.

Finally, this work has helped recognise a whole host of potential electromagnetic applications that nonwoven materials could be developed for. These not only include shielding applications, but also a range of current carrying requirements (including resistive heating and lightning strike protection).

6 Future work

There are plenty of opportunities to further the work in this field. Work that is of particular interest to this project are listed below, however they are by no means the remaining areas of research and development.

6.1 TRL Calibration

Advanced 'Through Reflect Line' calibration standards allows for more accurate SE values to be inferred by removing signal noises phases changes and transmission loading. Some preliminary work has shown the benefits of such calibration – the rippled pink lines becoming the smoother blue lines.

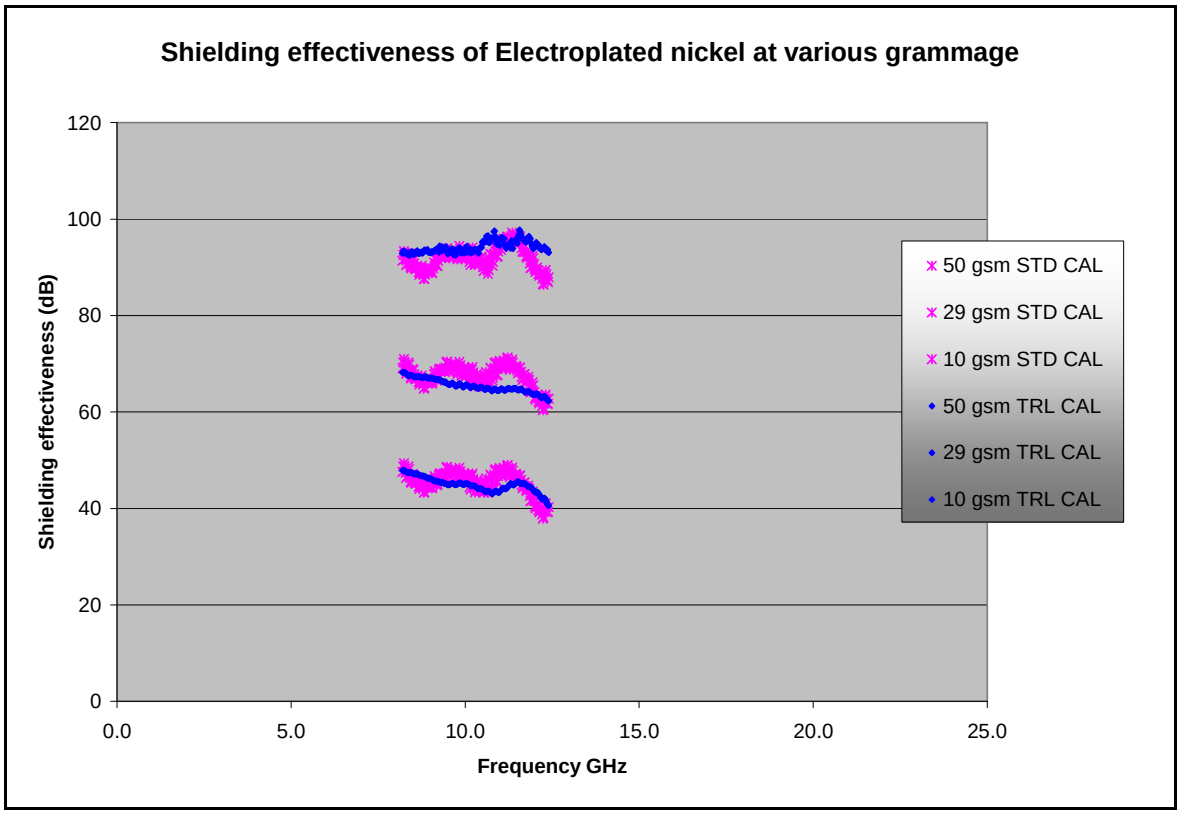

Figure 55: Advanced TRL calibrations can be used to remove the mismatch ripple (pink) and noise within the test setup

6.2 Measurements in the Far field

Far fields plane waves are more realistic of the real world applications in which nonwovens are incorporated. Therefore it is desirable to use a test method that replicated these conditions as closely as possible. In this study we only considered near field sources as **Figure 4** described.

However far field data is more difficult to obtain: specula reflections signal interference and edge effects are all much more difficult to control. Additionally to ensure that the test is carried out in the far field larger test setups are required. This isn't too greater a problem at frequencies 5 GHz and above, but for longer wavelength (lower frequencies) (1 GHz and below) test setups rapidly become very large!

6.3 Modelling

Most of the work in this report has concerned itself with SE measurement. The modelling of nonwoven materials both before and after they are incorporated into applications would evolutionise the product development process. However this is by no means an easy feat, even by modeller's standards.

The mapping of S-parameters (S12, S21, S11, S22) into the material properties σ, μ, ε requires careful inspection and manipulation. An array of algorithms is often used to perform this operation. Institutions such as BAE systems and Manchester University have spent year's refining these complex operations. Once a material's S-parameters and bulk properties have been quantified, the modelling of that material becomes a distinct possibility.

At this point, manipulation of S-parameters into material properties is beyond current understanding, and so whilst I continue my research, expertise in modelling will be pursued by consideration of ideal materials (such as Cu films), which have bulk properties which are already well defined.

Initial work has begun using too software packages: Mathcad 14 and Comsol Multi-physics. Although some initial results are presented here, a complete research programme would need to be committed in order to gain an accurate and usable model.

6.3.1 Mathcad 14

Mathcad 14 allows for a variety of mathematical based functions to be defined, manipulated and plotted and in a logical and efficient way. To date, shielding effectivness expressions have been defined and plotted in Mathcad, based on isotropic conductive films (copper). Tailoring the mathematical expressions towards TFP's materials may be quite straight forward, provided the bulk properties of the material has been quantified accurately.

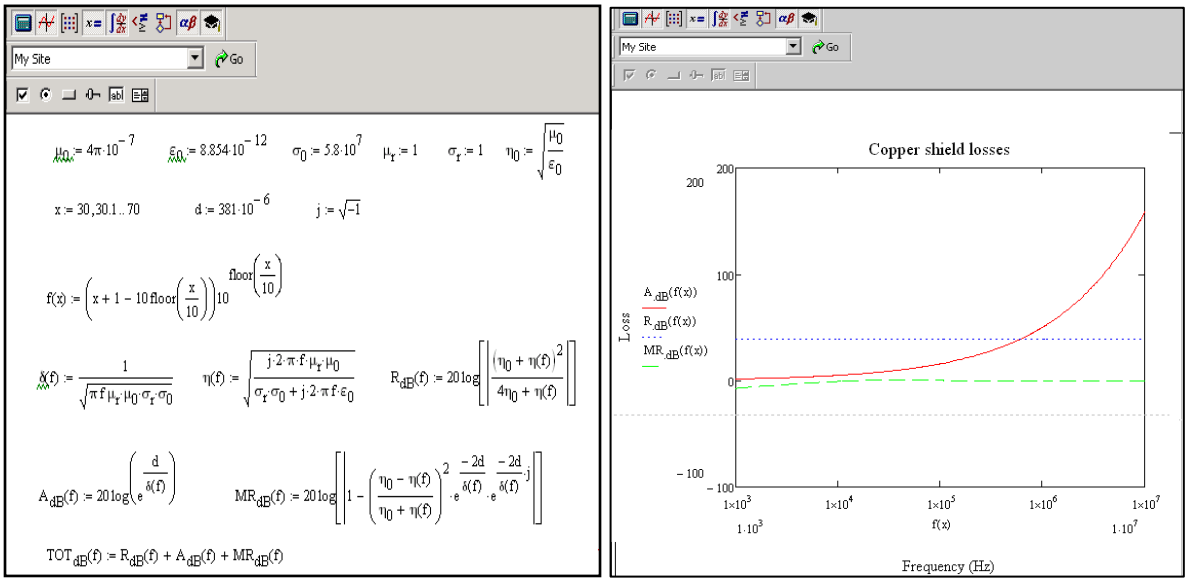

Figure 56: Operations in Mathcad: plotting the mechanisms of SE at different frequencies.

It should be realised that Mathcad 14 is an effective and efficient graph plotting tool. It allows us to model responses and parameter evolution, but it is not an integrated modelling package such as Comsol. It does however provide an effective stepping stone into the modelling world.

6.3.2 Comsol Multiphysics

Modelling of the nearfield (waveguide) technique.

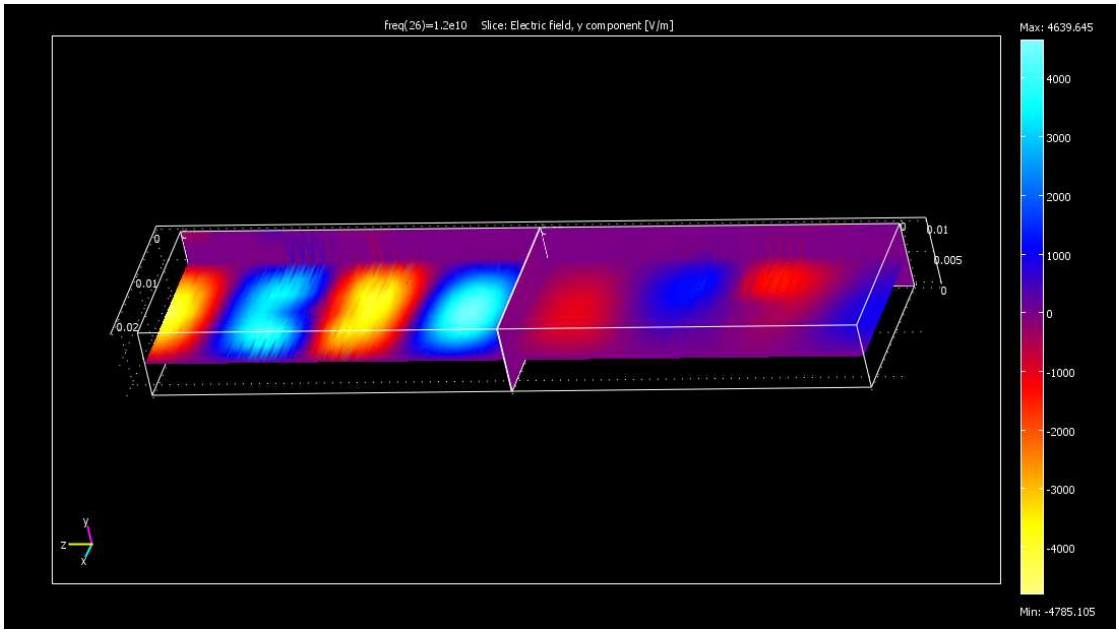

Figure 57: In this simple Comsol model, a transverse electric wave illuminates a material (placed at the centre of the test cell). The model approximates the types of nearfield boundary conditions that are present in nearfield waveguide testing.

This model was designed to replicate the shielding effectiveness test method that is currently being used to generated nearfield results in this report. As the electric field passes through the material (*left to right*) the magnitude of the field is reduced as once would expect for a shielding material. Such reduction (or attenuation) is proportional to the relative bulk properties of the material ($\sigma / \mu / \varepsilon$) which can be defined within the model, as can frequency, temperature and many more factors.

6.4 Alignment

By altering the manufacturing process, the polarisation of fibre within the nonwoven structure is possible. Preliminary results have shown alignment ratio's of up to 100/1[H]. This could benefit certain applications in which frequencies of a certain polarisation are unwanted and require filtering. Figure 58 compares two aligned materials against two isotropic materials

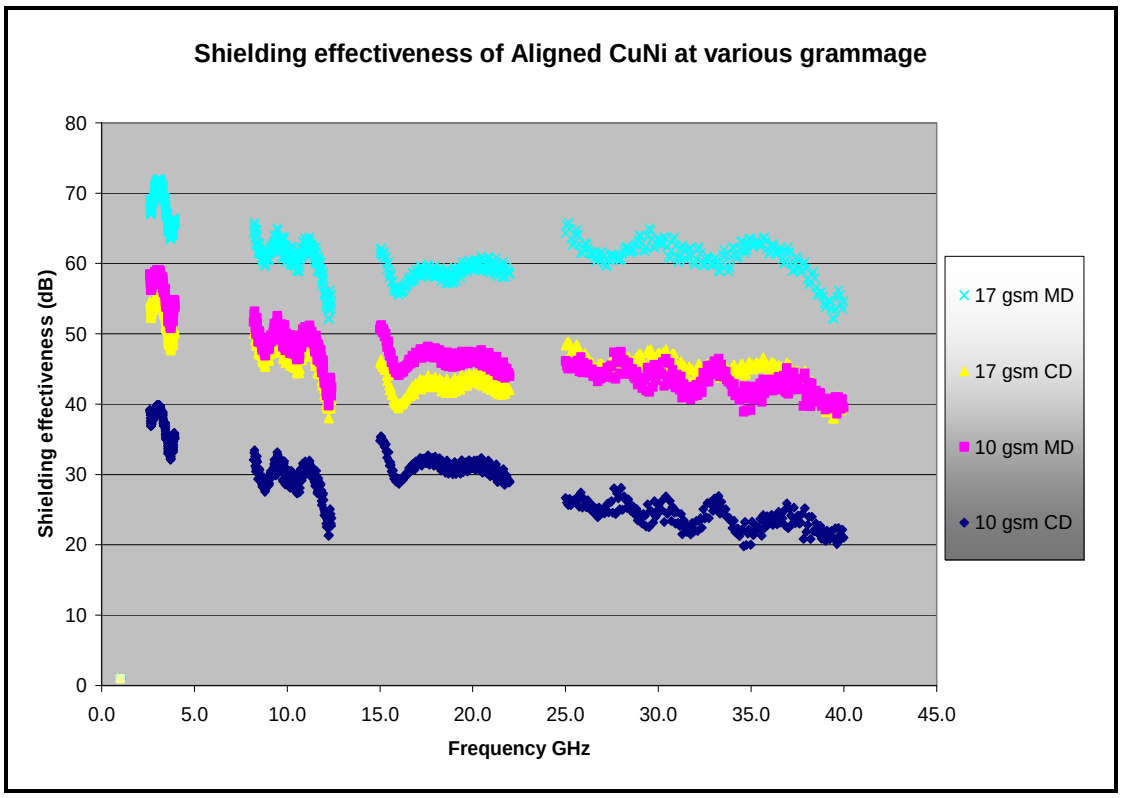

Figure 58: The effects of aligning the fibre matrix that makes up the nonwoven veil.

As can be clearly seen in the diagram above, fibre alignment has produced a greater SE in the same plane as the signal (MD) - approximately a 15dB boost in the SE can be seen. By the same principle, the converse is true of the materials aligned at 90 degrees to the signal plane (CD). This demonstrates the kinds of potential that fibre alignment can bring.

[H] Based on tensile testing ratios: materials are strong in the machines direction than the cross direction.

6.5 Thickness effects

The thickness of the sample can have a large impact on the mechanisms that govern shielding. To understand this more precisely a study into the SE of different thickness materials is required. Both thicker and thinner nonwoven sub straights would be interesting to look at (for aerospace and mobile phone applications respectively).

One challenge in testing thicker nonwoven materials is that they are compressible and so ensuring that the manufactured, tested and applied product thickness remained constant is important. For thinner nonwoven materials (which can be achieved via various calandering operations) there are equal concerns. There are that the calendaring process can damage the properties of the fibres, for example the surface micro-cracking of the metal coatings my compromise performance. However this will remain unanswered until preliminary testing has taken place.

7 Appendices

7.1 Typical 'everyday' electric and magnetic fields

Electric fields			Magnetic fields	
Electric appliance	**Electric field strength (V/m)**		**Electric appliance**	**Magnetic field strength (μT)**
Stereo receiver	180		Hair dryer	0.01 – 7
Iron	120		Electric shaver	0.08 – 9
Refrigerator	120		Vacuum cleaner	2 – 20
Mixer	100		Fluorescent light	0.5 – 2
Toaster	80		Microwave oven	4 – 8
Hair dryer	80		Portable radio	1
Colour TV	60		Electric oven	0.15 – 0.5
Coffee machine	60		Washing machine	0.15 – 3
Vacuum cleaner	50		Computer	< 0.01
Electric oven	8		Refrigerator	0.01 – 0.25
Light bulb	5		Colour TV	0.04 – 2
Guideline limit value	**5000**		**Guideline limit value**	100 μT

Figure 59: Typical EM fields every day items (based on a distance 30cm)[17]

7.2 Network Analyser 'Through' calibration method.

1. Set frequency range to be tested
2. Set the power to 10dBm
3. In channel select 'Measure bandwidth'. Choose a power band average of 1 KHz
4. Connect the coaxial cable to both the network analyser and waveguides. Clamp the waveguides together using the vice.
5. On the Network Analyser, in channel select 'CAL' > start CAL
6. Select the calibration kit used and connector > tick box Short (m)…
7. A measurement should be initiated, with the Network Analyser performing multiple calibration sweeps.
8. A green check mark should result in the check box.
9. To finish the calibration click Apply.
10. The Network Analyser should now display a 0dB shielding level.

Once calibrated as above, the network analyser will record 200 results per measurement. This enables 3600 results to be taken per sample for the whole frequency range.

7.3 CSV file processing

The guide below describes the method that should be applied when trying to format raw data from the network analyser into an excel spread sheet. The step is necessary as raw data is initially presented as 'comma separated value' (CSV) files. These images complement the in text guide.

A)

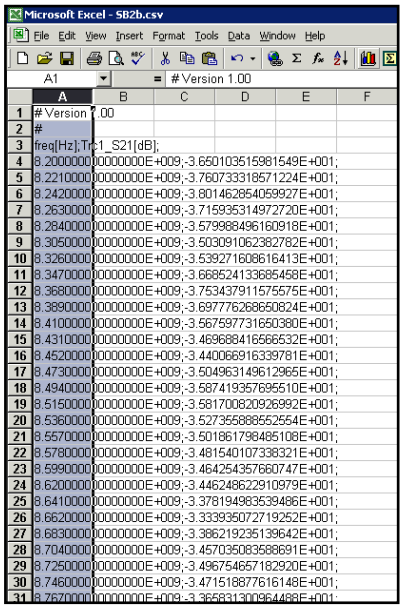

B)

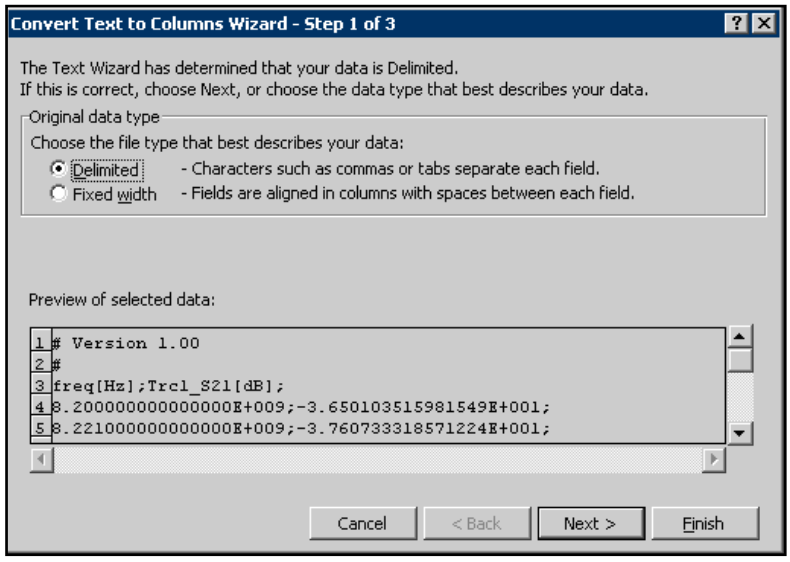

C)

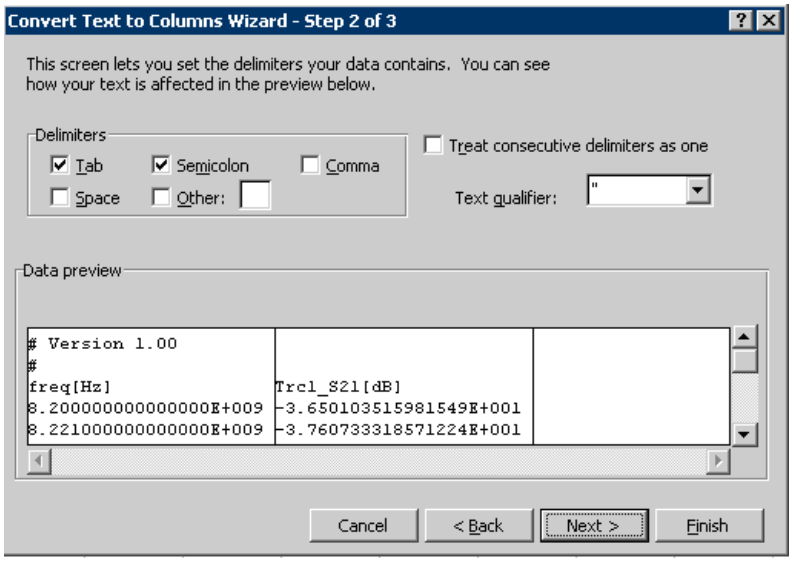

D)

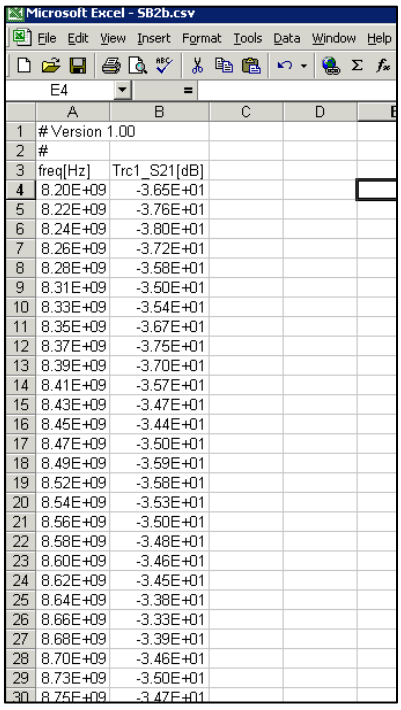

7.4 Production of nonwoven materials in the laboratory

(Metal particle impregnation work).

The manufacture of laboratory produced samples for metal particle inclusion is provided below.

A 12” hand sheet maker is used to drain a fibrous dispersion over a porous membrane. The fibres are deposited onto this membrane whilst the remaining solution is drained away. This solution is largely made up of water, viscosity modifier and binding ingredients.

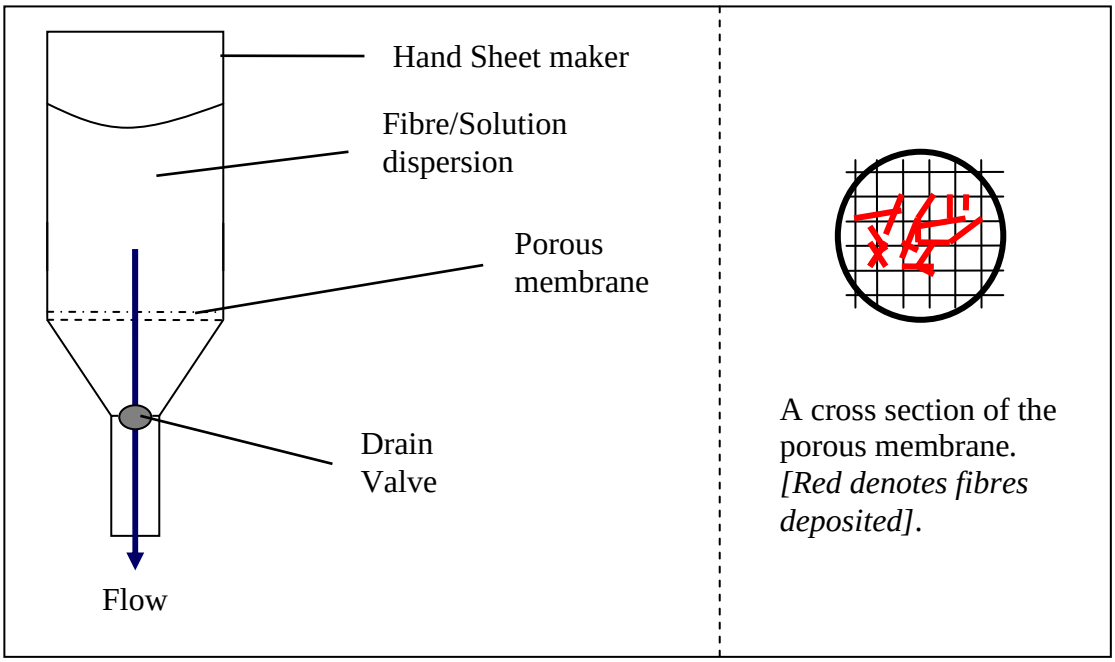

Figure 60: The handsheet maker: allowing for the manufacture samples in the laboratory.

The resulting web of fibres is then transferred to a drying oven, activating the polymer binder. By altering the amounts of fibre added to the handsheet maker, its possible to control the basis weight of the material. Once dry base sheets are then coated with the relevant metal type using a syringe and roll method and then re-dried in a solvent oven. The full procedure is detailed below.

The following components were added to the 12 inch handsheet maker:

Industrial blender – 21ml texipol/3 litres of water	x2	Blended for 1 minute
Philips blender – 7ml texipol/1 litre of water	x1	Blended for 1 minute

The 6mm Nickel coated carbon fibre is added and blended in the Philips blender along with Texipol solution for 1 minute. A 5% addition of Kurraray (PVOH) binder was added to help give the samples some wet strength so that they could be successfully transferred to the oven for drying.

The hand sheet is then coated using a syringe and roll technique. It was necessary to produce a suspension of metal, which could then be syringed on to the base sheet. A polyester binder (Hexion WD30) was added to a Texipol solution to produce this suspension *(binder added to fuse the particles into the sheet after application).*

Addition of a wetting agent (Hydropalat 883) to some metal powders (Goldbronze 3001/3002) was necessary as the surface tension of the solution was preventing the powders to enter suspension.

The coated handsheet was then dried in the solvent oven for ~ 1 hour at $100\,°c$.

8 Bibliography

A. Stutzman, W. & Thiele, G., 1981. *Antenna Theory and design.* New Jersey: Wiley.

B. Ulaby, F., 1997. *Fundamentals of applied Electromagnetics.* New Jersey: Prentice Hall.

C. Grant, I. & Phillips, W., 1990. *Electromagnetism.* 2nd ed. New Jersey: Wiley.

D. Ghodgaonkar, D., 2000. *Microwave Nondestructive Testing of Composite Materials using Free-Space Microwave Measurement Techniques.* Available at www.ndt.net/article/wcndt00/papers/idn251/idn.htm [Accessed 23 April 2009].

E. Clarke, B. et al., 2003. *A guide to characterisation of dielectric materials at RF and Microwave frequencies.* London: National Physics Laboratory.

F. Morgan, P., 2005. *Carbon Fibres and their Composites.* Florida: CRC Press.

G. Kaiser, K., 2006. *Electromagnetic Shielding.* Florida: CRC Press

H. Paul, C., 2006. *Introduction to Electromagnetic Compatibility.* 2nd ed. New Jersey: Wiley.

I. Hiebel, M., 2008. *Fundamentals of Vector Network Analysis.* 4th ed. Munchen: Rohde & Schwarz.

J. Vasquez, H. Espinoza, L. Lozano, K. Foltz, H & Yang, S,. 2008. *Simple device for Electromagnetic Interference Shielding Effectiveness Measurement. 26th August IEEE, pp. 62-68.*

9 References

[1] Austin, A., 2009 *Manufacture and evaluation of hybrid carbon nanofibre containing nonwoven papers,* SAMPE conference paper pp. 8 – 9.

[2] Ladkin, P., *Electromagnetic interference with aircraft systems: why worry?* [Online] Available at: www/rvs.unibielefeld.de/publications/incidents/docs/research/rvs/article/emi.html. [Accessed 12 December 2009]

[3] Berger, A., 1997 *Personal communication.*

[4] V Vasquez, H. Espinoza, L. Lozano, K. Foltz, H & Yang, S,. 2008. *Simple device for Electromagnetic Interference Shielding Effectiveness Measurement. 26th August IEEE, pp. 62-68.*

[5] Sim, C.,2002 *Standards in Defence News Electromagnetic interference,* DSTAN UK Defence Standardisation

[6] Scarry, E. 1998. *The fall of TWA 800: The possibility of electromagnetic interference* NYRB

[7] Chittenden, M. 2007. *Is it the phone mast's fault? The Times online, [internet] Available at:* http://www.timesonline.co.uk/tol/news/uk/article1687357.ece. [Accessed 3 January 2010].

[8] The Health Protection Agency, 2009 Available at: *http://www.hpa.org.uk/webw/HPAweb&HPAwebStandard/HPAweb_C/.*

[9] Association of the Nonwovens Fabrics industry (INDA),. 2009. *About Nonwovens.*[Online]. Available at: http://www.inda.org/about/nonwovens.html [Accessed 23 July 2009].

[10] Cyber Physics., 2008. *The Electromagnetic Spectrum: The family of light.* [Online] Available at: *http://www.cyberphysics.co.uk/topics/light/emspect.htm* [Accessed 19 August 2009].

[11] Vision Learning., 2007. *Light II: Electromagnetism.*[Online]Available at: http://www.visionlearning.com/library/module_viewer.php?mid=138 [Accessed 3 December 2009]

[12] Marvin, A., 2009. *Principles of Engineering Electromagnetics.* York EMC Services.

[13] Sweetman, B,. 1986. *Stealth Aircraft, secrets of future airpower*. Belfast: Airlife Publishing Ltd.

[14] Bekaert Fibre Technologies., 2008. Available at ***www.bekaert.com*** [Accessed 21 September 2009]

[15] Wieckowski,. T .2006. *Methods* for evaluating the shielding effectiveness of Textiles. *Fibres & Textiles in Eastern Europe* 14(5), pp. 18-22.

[16] See reference 1.

[17] The World Health Organisation (WHO),. 2010 Available at: *www.who.int/peh-emf/about/WhatisEMF/en/index3.html [Accessed 15 June 2009]*